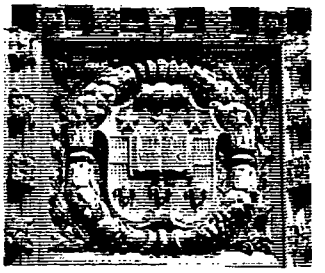

# WASHINGTON UNIVERSITY

REPORT No. (R)T-72/2 SEPTEMBER, 1972



## A WIDEBAND 12 GHz DOWN-CONVERTER

BURTON A. NEWMAN

FRED J. ROSENBAUM

WASHINGTON UNIVERSITY / ST. LOUIS / MISSOURI 63130

PROGRAM ON APPLICATION OF COMMUNICATIONS SATELLITES
TO EDUCATIONAL DEVELOPMENT

CENTER FOR DEVELOPMENT TECHNOLOGY

WASHINGTON UNIVERSITY

Report No. (R)T-72/2 September, 1972

# A WIDEBAND 12 GHz DOWN-CONVERTER

Burton A. Newman

Fred J. Rosenbaum

This research is supported by the National Aeronautics and Space Administration under Grant No. Y/NGL-26-008-054. This memorandum is primarily for internal distribution and does not necessarily represent the views of either the research team as a whole or the National Aeronautics and Space Administration.

# A WIDEBAND 12 GHz DOWN-CONVERTER

## ABSTRACT

The design, fabrication, and evaluation of a single ended 12 GHz down-converter suitable for use in a low cost satellite ground terminal is described. The mixer uses waveguide, coaxial and MIC (microwave integrated circuit) transmission line components. The theoretical and experimental analysis of several microstrip circuit elements is presented including the traveling wave-directional filter, quarter wavelength proximity directional coupler, low pass filter and the quarterwave band stop filter. The optimum performance achieved for the mixer using a packaged diode was 9.4 dB conversion loss and a bandwidth of 275 MHz.

TABLE OF CONTENTS

TABLE OF CONTENTS
(continued)

# LIST OF TABLES

## LIST OF FIGURES

LIST OF FIGURES
(continued)

# A WIDEBAND 12GHZ DOWN-CONVERTER

## 1. INTRODUCTION

### 1.1 BACKGROUND

In the development of an educational communication system, the satellite is seen as a cost effective and technically feasible transmission link. (1)* In conjunction with a CATV distribution system, a large number of TV-equivalent bandwidth channels could be provided to disseminate the vast amount of material required by educational subscribers. In a previous study (1), it was suggested that the satellite-CATV interconnection might use moderately priced earth-terminals capable of multiple carrier reception, utilizing one RF carrier for each TV channel. The multi-carrier system allows for the origination of individual programs from different points, a necessary feature for an interactive system.

As part of this program, the first element of this system, the downconverter, has been designed, fabricated

*The numbers in parentheses in the text indicate references in the Bibliography.

and tested. The required specifications were determined in a study by Singh (2). The specifications actually achieved are reported throughout the succeeding chapters and are summarized in the concluding chapter. In order to give perspective into this problem area, some of the recent work reported is summarized here.

## 1.2 PREVIOUS RESULTS

Lusignan et al. (3) describe a 2.5GHz waveguide balanced-mixer low-cost receiver with a design goal of 9db noise figure. The receiver bandwidth is 40MHz. The suggested local oscillator is a cavity mounted Gunn diode. A 100KHz video guard band would be required if the LO is operated without phase locking. No AFC loop was described in this report. The balanced mixer is proposed to eliminate the expected large AM noise component from the Gunn diode. Previous work done at Washington University (4-9) indicates that they should be very good LO's with lower AM noise than even "low noise" klystrons.

General Electric has also reported on a single channel 40MHz bandwidth X-band receiver (10). The balanced mixer was implemented in stripline and used ultrasonically bonded beam-lead diodes. The input bandpass filters had a midband insertion loss of 3db. A noise figure of 11.0 ± .1db was measured (including the IF amplifier) with an LO power of 5dbm. A Varian VSX-9001 Gunn oscillator yielded an uncompensated frequency stability of about

200KHz/°C. Addition of a temperature compensating alumina probe reduced the drift to less than 20KHz/°C. A 15db gain transistor IF amplifier was used. It had a 150MHz bandwidth and a 3db noise figure.

An X-band microstrip mixer using GaAs Schottky Barrier Diodes which used a 500MHz thin film IF preamplifier was reported by K. M. Johnson (11). The balanced mixer used filters to terminate the image frequency in a short circuit at the diode. The thin film IF amplifier had a 2.2db noise figure. The total mixer noise figure was 6.7db.

RCA Laboratories (12) developed a low noise (6.4db) X-band receiver with a total signal gain of 39db. The 500MHz IF amplifier had a 540MHz bandwidth and a 3db noise figure.

Oxley (13) has described an X-band receiver using planar GaAs Schottky Barrier Diodes in a balanced mixer configuration. A 6db noise figure was obtained.

Westinghouse (14) reported results at 9.5GHz using a single-ended mixer and a 1GHz IF. A conversion loss of 4db was achieved using a GaAs chip diode and sum and image frequency recovery techniques. Further results (15,16) in addition to those above are summarized in Table 1.

The Washington University 12GHz down-converter described herein uses waveguide, coaxial, and microstrip transmission line elements. Necessary filtering is done exclusively in microstrip for reasons to be explained later. The mixing

Table 1. Performance Characteristics of X-Band Receivers.

| COMPANY | WAVE-GUIDE OR IC | BALANCED OR SINGLE | IMAGE | DIODE | fs(GHz) | IF(MHz) | BAND-WIDTH (MHz) | CON-VERSION LOSS (db) | IF NOISE FIGURE (db) | SYSTEM NOISE FIGURE (db) |
|---|---|---|---|---|---|---|---|---|---|---|
| Texas Inst.(11) | IC | Bal. | Open | GaAs | 9 | 500 | 200 | 4 | 2.2 | 6.3 |
| RCA (12) | IC | Bal. | - | Glass Pack. SBD | 9 | 500 | 540 | 6 | 3 | 7 |
| G.E.C.(13) Semicon-ductors | IC | Bal. | - | GaAs SBD | 9.375 | 45 | 20 | - | 2 | 7.5 |
| Westing-house (14) | IC | Single | Open | GaAs SBD | 9.5 | 1000 | 450 | 3.5 | - | - |
| Bell Labs (15) | WG | Bal. | - | GaAs SBD | 10.76 | 300 | 120 | 3.6 | 2 | 5.6 |
| Tele- (16) funken | IC | Bal. | - | Beam Lead | 12 | 650 | 300 | 8 | - | 12 |
| Philips (16) | IC | Bal. | - | Beam Lead | 12 | 70 | 30 | - | - | 7 |
| NHK (16) | WG | Single | Open | GaAs SBD | 12 | 650 | 300 | 2.8 | - | - |

process itself occurs in a coaxially mounted Schottky Barrier Diode. The diode cavity was designed so as to accommodate both ceramic cartridge and pill-prong mounted Si and GaAs diodes, respectively.

Section 1.4 of this chapter considers the mixing process itself. The diode DC i-v characteristic will be approximated by a simple exponential curve to illustrate the mathematical origin of the various frequency components.

## 1.3 SCOPE

Chapter 2 is concerned with microwave propagation in microstrip and how this knowledge can be applied to device design. This is followed by an analysis and experimental results for a directional coupler, a lowpass filter and a traveling-wave directional filter. The section concludes with some data taken for a band-stop filter.

Chapter 3 develops the rationale for the specific design choices that were made. Included are early crystal holder results and the transition to the final package design. Justification for the final microstrip circuit is given and mismatch data for the unmounted board is presented.

Performance data for the developmental down-converter is given in Chapter 4. Final discussion and summarized results can be found in the concluding Chapter 5.

## 1.4 MIXED FREQUENCY SPECTRUM

As an introduction to the X-band down-converter reported here, we first consider the mixing process. The

DC i-v characteristic of an idealized mixer diode is given by:

$$I = I_s(e^{qV/nkT} - 1) = I_s(e^{\alpha V} - 1) \qquad (1.1)$$

where:

$I_s$ = diode saturation current

$q$ = electronic charge

$V$ = voltage across the junction

$n$ = constant ≈ 1

$k$ = Boltzman's constant

$T$ = absolute temperature

$\alpha$ = $q/nkT$

Now, expanding the current as a Taylor expansion about the DC level $V_o$ leads to

$$I = I(V_o) + \delta V\frac{dI}{dV} + \frac{1}{2}\frac{d^2I}{dV^2}(\delta V)^2 + \text{higher order terms} \qquad (1.2)$$

when

$$\frac{dI}{dV} = \alpha I_s e^{\alpha V_o} \qquad (1.3)$$

$$\frac{d^2I}{dV^2} = \alpha^2 I_s e^{\alpha V_o}$$

These quantities can be measured directly around the operating point of a diode i-v characteristic (see Figure 19). And,

$$\delta V = V_{LO} + V_{SIG} = V_L \cos\omega t + V_S \cos(\omega+\beta)t \qquad (1.4)$$

with

$\omega$ = local oscillator (LO) radian frequency

$\omega+\beta$ = signal radian frequency

Also,

$$(\delta V)^2 = \left\{V_L \cos\omega t + V_S \cos(\omega+\beta)t\right\}^2 \qquad (1.5)$$

$$= V_L^2 \cos^2\omega t + V_S^2 \cos^2(\omega+\beta)t + 2V_L V_S \cos(\omega t)\cos(\omega+\beta)t$$

$$= \frac{V_L^2}{2}(1 + \cos 2\omega t) + \frac{V_S^2}{2}(1 + \cos 2(\omega+\beta)t) + V_L V_S(\cos\beta t + \cos(2\omega+\beta)t)$$

Equation (1.5) yields a DC component plus the intermediate frequency (IF) and the sum frequency in addition to the second harmonics of the LO and signal. The above process has been simplified in several major respects:

1. Only the fundamental LO frequency was considered.
2. Only second order terms were considered in the transfer characteristic.
3. Only the first mixing components were considered, i.e., the frequencies produced by the first mixing in turn mix with the original LO and signal frequencies in addition to each other. Obviously the physical process is a good deal more complicated than that described above.

A final correction must be mentioned. The transfer characteristic given is that for a diode exhibiting an ideal

exponential i-v characteristic. A rigorous derivation by Barber (17) allows for the more realistic situation of a non-ideal exponential i-v characteristic in addition to a non-sinusoidal pumping waveform.

## 2. FILTER FABRICATION IN MICROSTRIP

### 2.1 MICROWAVE PROPAGATION IN MICROSTRIP

As mentioned in the introduction, microstrip was chosen as the medium to be used for the design of the various filter networks of the mixer. Requisite to the design of such devices is a knowledge of microwave propagation on microstrip specifically including such parameters as characteristic impedance, velocity of propagation, and capacitance. The above characterization has been well established in the literature (18-21).

For the design of devices with more than two ports, the even and odd mode normal impedances and velocities of coupled pairs of microstrip lines must be known. Bryant and Weiss (18) have presented a solution to the problem in the "quasi-static" limit valid for propagation in the low gigahertz region.

Consider the pair of coupled microstrip transmission lines in Figure 1. The characteristics of the structure are usually specified as functions of the parameters W/H, S/H and K, where W is the strip width, H is the thickness of the dielectric, S is the space between the strips and K is the relative dielectric constant. The strip thickness is assumed to be infinitesimal.

The electrostatic problem is then solved rigorously for the capicitance of single and coupled strips on a

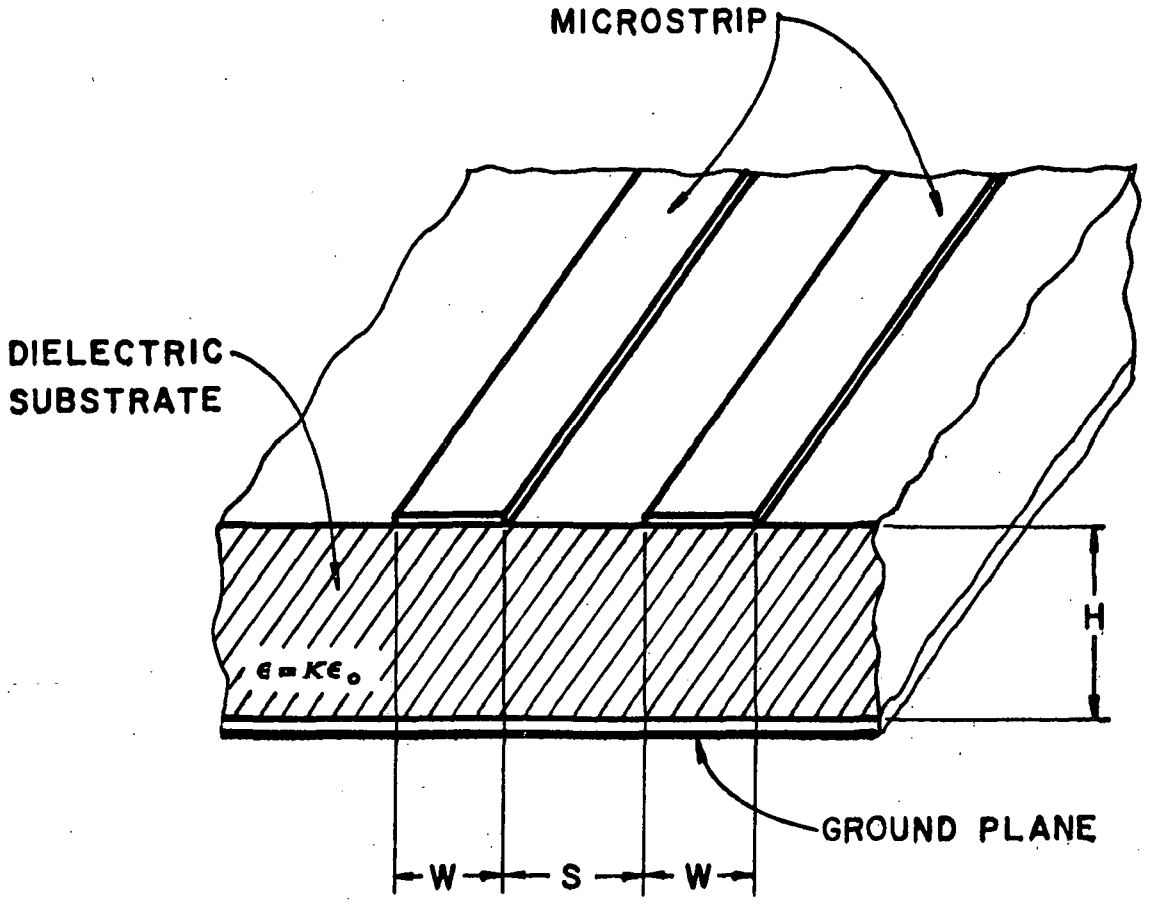


Figure 1. A Coupled Pair of Microstrip Lines.

dielectric substrate. This solution can then be applied to the case at hand, that is, propagation at microwave frequencies, by assuming a negligible longitudinal field component, thus yielding a TEM solution.

Referring to Figure 1, both strips are at a potential V for even mode propagation and have opposite signs but equal magnitude for odd mode propagation. Coupling occurs for odd mode propagation only. After the charge and potential distributions have been determined from the field configurations, the capacitance per strip $C_K$ can be found, where $C_K = Q/V$, and Q is the given charge distribution. Note that the above charge and potential distributions are that of a nonhomogeneous boundary value problem, a bounded dielectric substrate and free space above. This implies the need for an effective relative dielectric constant.

The effective dielectric constant of the medium, $K_{eff}$, can then be given as $K_{eff} = C_K/C_O$ where $C_O$ is the capacitance for the case of microstrip in vacuum. This parameter is necessary for the determination of the wavelength in the given medium, $\lambda_{K_{eff}} = \lambda_o/\sqrt{K_{eff}}$, where $\lambda_o$ is the free space wavelength. Similarly, the velocity of propagation in the medium is given by $v = c/\sqrt{K_{eff}}$ where c is the speed of light in vacuum. Finally, the characteristic impedance of the medium $Z_o$ may be calculated as

$$Z_o = \frac{1}{vC_K} = \frac{1}{cC_o\sqrt{K_{eff}}} \qquad (2.1)$$

## 2.2 DIRECTIONAL COUPLER

Given the characteristic impedance, velocity of propagation and effective dielectric constant for coupled microstrip transmission lines, standard microwave devices may now be designed. One of the primary tasks in the design of a mixer that must be immediately identified is that of combining the signal frequency and the local oscillator or pump. Several configurations are available for this duty. Two will be described in this chapter. The first to be discussed is the directional coupler.

### 2.2.1 Design and Analysis

The directional coupler is a four-port device that has the following properties (22). Referring to Figure 2, a wave incident in port 1 couples power into ports 2 and 3 but is isolated from port 4. Similar relations hold for combinations of the other ports. The device is also characterized by the fact that if three ports are terminated in matched loads, the fourth port will also be matched to an incident signal. Since directional couplers are bandlimited devices, two parameters can be defined to express performance as a function of frequency. The coupling C is given by:

$$C = 10 \log \frac{P_i}{P_f} \text{ db} \qquad (2.2)$$

where $P_i$ is the incident power and $P_f$ is the power coupled in the forward direction.

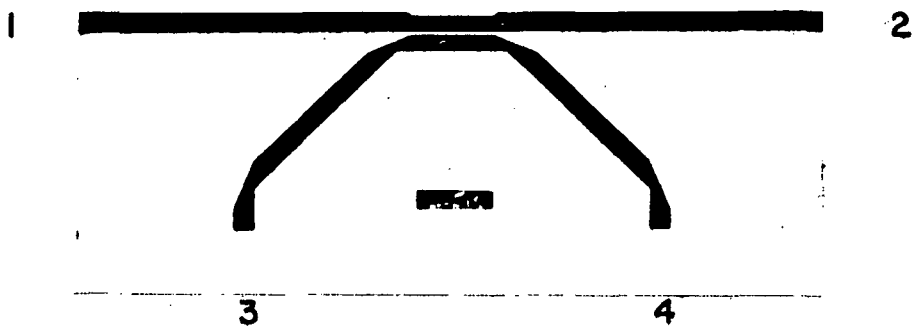


Figure 2. Microstrip Directional Coupler Mask.

The directivity D(db) is given by:

$$D = 10 \log \frac{P_f}{P_b} \tag{2.3}$$

where $P_b$ is the power coupled to the "isolated" port. Its scattering matrix (22) is:

$$[S] = \begin{bmatrix} 0 & c_1 & jc_2 & 0 \\ c_1 & 0 & 0 & jc_2 \\ jc_2 & 0 & 0 & c_1 \\ 0 & jc_2 & c_1 & 0 \end{bmatrix} \tag{2.4}$$

where $c_2 = (1 - c_1^2)^{1/2}$.

The microstrip device used for the receiver can be accurately described as a TEM-mode, backward-coupled directional coupler. As mentioned above, the coupler performance is frequency sensitive. The midband coupling length is designed to be 90°. It should be noted here that although multisection devices can be designed to increase the bandwidth, it was felt that the present system requirements could be satisfied by a single section coupler.

The following relations (23) will be used to derive expressions for the coupling and directivity as functions of frequency:

$$\frac{E_3}{E_1} = \frac{jc \sin\theta}{\sqrt{1 - c^2}\cos\theta + j \sin\theta} \tag{2.5}$$

where

$\frac{E_i}{E_1}$ = voltage at port i, $i \neq 1$.

$j = \sqrt{-1}$

$c = c_1$ = coupling factor, midband value of $|E_3/E_1|$

c also equals antilog (C/20).

$\theta$ = phase length of coupling section.

Also,

$$\frac{E_2}{E_1} = \frac{\sqrt{1 - c^2}}{\sqrt{1 - c^2}\cos\theta + j \sin\theta} \tag{2.6}$$

Expressing Equations (2.5) and (2.6) as power ratios, we have

$$\left|\frac{E_3}{E_1}\right|^2 = \frac{c^2 \sin^2\theta}{1 - c^2\cos^2\theta} \tag{2.7}$$

$$\left|\frac{E_2}{E_1}\right|^2 = \frac{1 - c^2}{1 - c^2\cos^2\theta} \tag{2.8}$$

The coupling factor C of Equation (2.2) is just

$$C = 10 \log |E_1/E_3|^2. \tag{2.9}$$

The directivity of Equation (2.3) is given by:

$$D = 10 \log |E_3/E_4|^2 = \infty \tag{2.10}$$

Notice that Equations (2.5) through (2.10) assume that the impedances at each port are equal for all frequencies. For the ideal theory above, the "isolated" port voltage and power are predicted to be zero. It will be shown later that the power from the fourth, isolated, port is dependent on the mismatch occurring at the other three ports.

Matthaei, et al. (23) have shown that the coupling factor c can also be expressed as a function of the even and odd mode impedances ($Z_{oe}$ and $Z_{oo}$, respectively):

$$c = \frac{Z_{oe}/Z_{oo} - 1}{Z_{oe}/Z_{oo} + 1} \tag{2.11}$$

In order to obtain a match at the input, the characteristic impedance of the coupling section must be adjusted to:

$$Z_o = \sqrt{Z_{oe}Z_{oo}} \tag{2.12}$$

The fact that the odd mode occurs when equal and opposide currents are flowing in the coupled microstrip lines illustrates the "backward coupling" phenomenon.

Equations (2.11) and (2.12) can be rearranged to yield the following design relations:

$$\begin{aligned} Z_{oe} &= Z_o\sqrt{\frac{1 + c}{1 - c}} \\ Z_{oo} &= Z_o\sqrt{\frac{1 - c}{1 + c}} \end{aligned} \tag{2.13}$$

As mentioned above, the ideal theory for the directional coupler assumes perfect isolation for the uncoupled port. In practice, this port does have a power output. It will now be shown that its power output and the overall directional coupler performance are dependent on the matches at each port.

It is well known that the input and output voltage waves of a device are related through its characteristic scattering matrix. Let $V_i^+$ and $V_i^-$ represent the input and

output waves respectively at the $i^{th}$ port, and let $\Gamma_i$ be the reflection coefficient where

$$\Gamma_i = \frac{V_i^+}{V_i^-} .$$

The voltage waves at the four ports can then be related as follows using the ideal direction coupler scattering matrix, Equation (2.4):

$$\begin{bmatrix} V_1^- \\ V_2^- \\ V_3^- \\ V_4^- \end{bmatrix} = \begin{bmatrix} 0 & c_1 & jc_2 & 0 \\ c_1 & 0 & 0 & jc_2 \\ jc_2 & 0 & 0 & c_1 \\ 0 & jc_2 & c_1 & 0 \end{bmatrix} \begin{bmatrix} 1 \\ \Gamma_2 V_2^- \\ \Gamma_3 V_3^- \\ \Gamma_4 V_4^- \end{bmatrix} \qquad (2.14)$$

For this analysis, reflection coefficients at the output ports are considered to be pure real. Equation (2.14) can be written:

$$\begin{aligned} V_1^- &= c_1\Gamma_2 V_2^- + jc_2\Gamma_3 V_3^- \\ V_2^- &= c_1 + jc_2\Gamma_4 V_4^- \\ V_3^- &= jc_2 + c_1\Gamma_4 V_4^- \\ V_4^- &= jc_2\Gamma_2 V_2^- + c_1\Gamma_3 V_3^- \end{aligned} \qquad (2.15)$$

These simultaneous equations can then be solved for the terminal voltages:

$$\begin{aligned} V_1^- = {} & c_1\Gamma_2\left\{c_1 - \frac{c_1 c_2^2 \Gamma_4(\Gamma_2 + \Gamma_3)}{1 - \Gamma_4(\Gamma_3 c_1^2 - \Gamma_2 c_2^2)}\right\} \\ & - c_2\Gamma_3\left\{c_2 + \frac{c_1^2 c_2 \Gamma_4(\Gamma_2 + \Gamma_3)}{1 - \Gamma_4(\Gamma_3 c_1^2 - \Gamma_2 c_2^2)}\right\} \end{aligned} \qquad (2.16)$$

$$V_2^- = c_1 - \frac{c_1 c_2^2 \Gamma_4(\Gamma_2 + \Gamma_3)}{1 - \Gamma_4(\Gamma_3 c_1^2 - \Gamma_2 c_2^2)} \tag{2.17}$$

$$V_3^- = j\left\{c_2 + \frac{c_1^2 c_2 \Gamma_4(\Gamma_2 + \Gamma_3)}{1 - \Gamma_4(\Gamma_3 c_1^2 - \Gamma_2 c_2^2)}\right\} \tag{2.18}$$

$$V_4^- = \frac{j c_1 c_2(\Gamma_2 + \Gamma_3)}{1 - \Gamma_4(\Gamma_3 c_1^2 - \Gamma_2 c_2^2)} \tag{2.19}$$

In this analysis a unit input voltage at port #1 was assumed to be the only external excitation.

2.2.2 Results

A microstrip directional coupler was fabricated and tested. Both theoretical and experimental results are shown in Figures 3 and 4. There are several significant points that should be mentioned concerning the fabricated device. Due to limitations in the microstrip fabrication capability of Washington University, strict line width tolerances could not be met. This resulted in three basic sources of experimental error.

The first is a variation of the characteristic impedance in both the single and coupled pair line sections. Also affected was the ability to predict coupling accurately across the coupled pair. Finally, due to restrictions on connector configuration and mask cutting technique bends were required resulting in rounding of the metalization at the corners. In sum, the above effects contribute to higher than desirable reflection coefficients at each port.

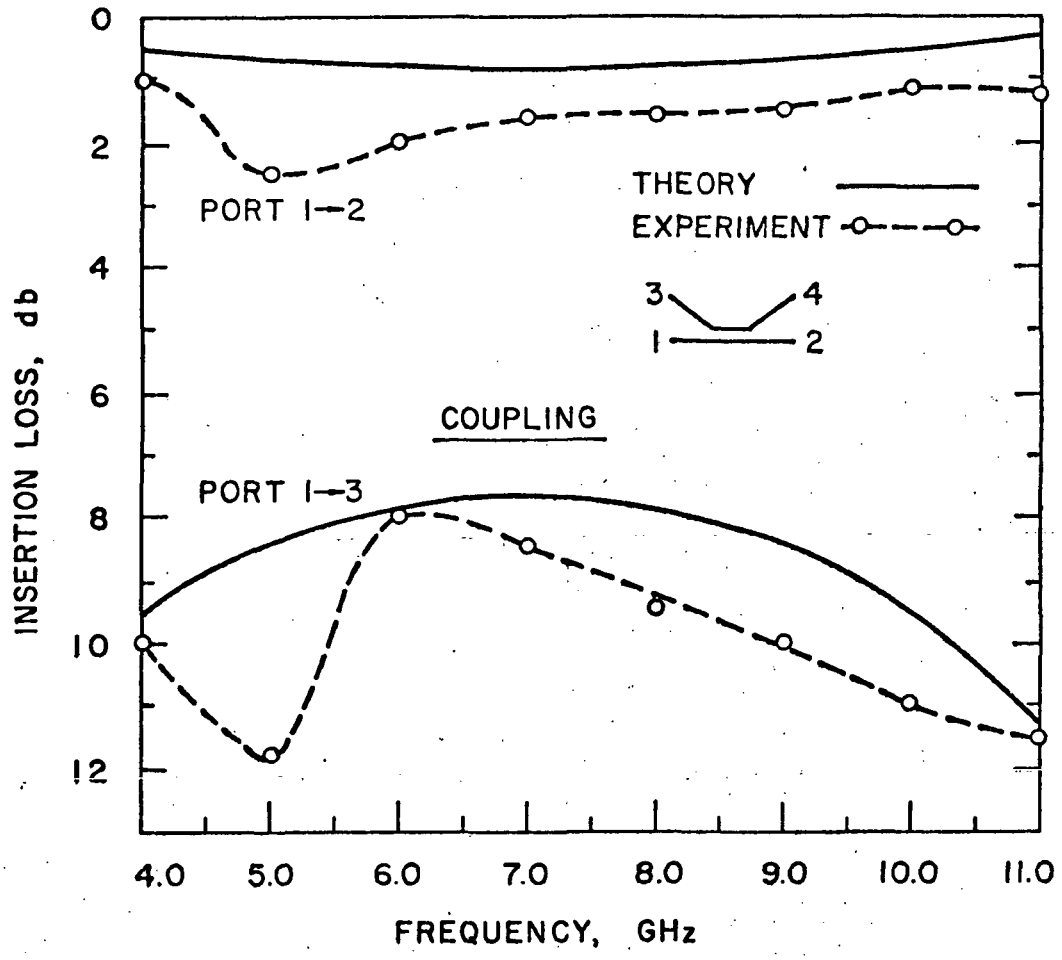


Figure 3. Directional Coupler "Coupling" Expressed as Insertion Loss from Ports 1→2 and 1→3 vs. Frequency.

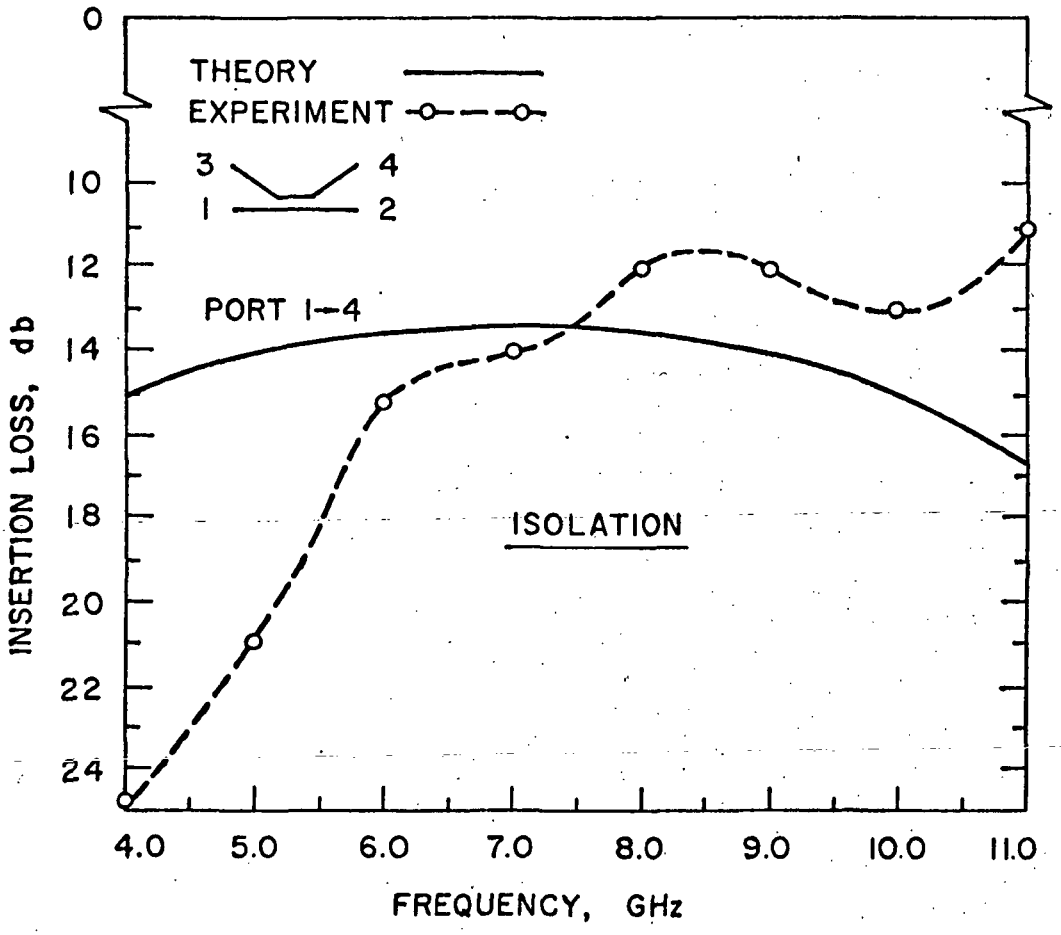


Figure 4. Directional Coupler Isolated Port Response Expressed as Insertion Loss from Port 1→4 vs. Frequency.

Theoretical results assuming identical mismatch at each port are shown in Figure 5 which demonstrate that a loss in isolation and consequent directivity can be expected as the port mismatches increase.

The theoretical results shown in Figures 3, 4 and 5 are based on the analysis given earlier in this section. In Figures 3 and 4, it is seen that the experimental points are generally speaking 1-1.5 db below the theoretical results. This is reasonable considering the approximate path length in microstrip ($\sim$ 1→1.5 inches) given the dielectric loss of microstrip of 1 db/inch.

The departures from expected experimental results are probably due to calibration and general experimental error in the reflectometer setup used to determine the device characteristic parameters.

Looking at Figure 4, it is seen that experimental and theoretical results do not coincide in any reasonable degree. Better agreement might result if the analysis had incorporated complex reflection coefficients rather than the assumed real values used here. However, the analysis was successful in predicting the general dependence of device performance on port mismatch. Specifically, it was shown that isolation is strongly dependent on reflection coefficient magnitude while coupling is generally unaffected.

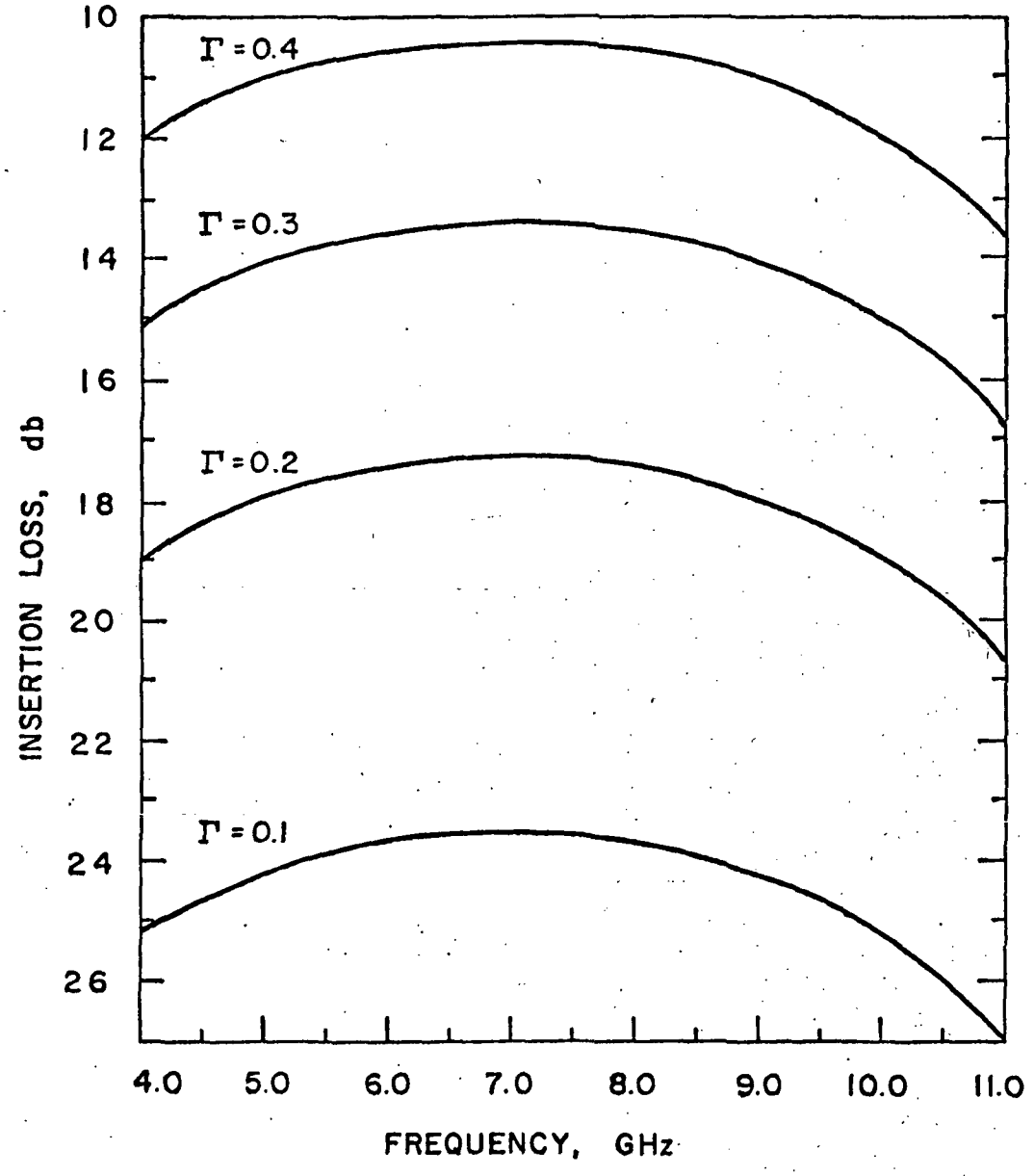


Figure 5. Directional Coupler Isolated Port Insertion Loss as a Function of Reflection Coefficient vs. Frequency for a 9 db Coupler.

## 2.3 LOWPASS FILTER

Another device that can easily be fabricated in microstrip is the low pass filter pictured in Figure 6. For the TEM mode filter considered here, the design is carried out by approximating an ideal lumped-element circuit such that individual elements are short compared to a quarter-wavelength at the pass-band frequencies (23).

### 2.3.1 Design and Analysis

Figure 7 shows the T and Π equivalent circuits of a length of nondispersive TEM transmission line. Note that this is an approximation for the dispersive microstrip medium.

If the line length, $\omega\ell/v$, is short compared to a quarter-wavelength then each section may be approximated by a single reactive element. A series inductance of $L = Z_o\ell/v$ henries can be simulated by a short length of high impedance line terminated at both ends by low impedances. Similarly, a shunt capacitance of $C = Y_o\ell/v$ can be simulated by a short length of low impedance line terminated by high impedance sections.

Although the above expressions allow for an adequate first order determination of the elemental values, several minor corrections can be applied at this point (23). Consider first the inductance of the high impedance section. A small negative correction to that value results from the inductance of the two adjoining low impedance sections. That is, for the $i^{th}$ inductive element:

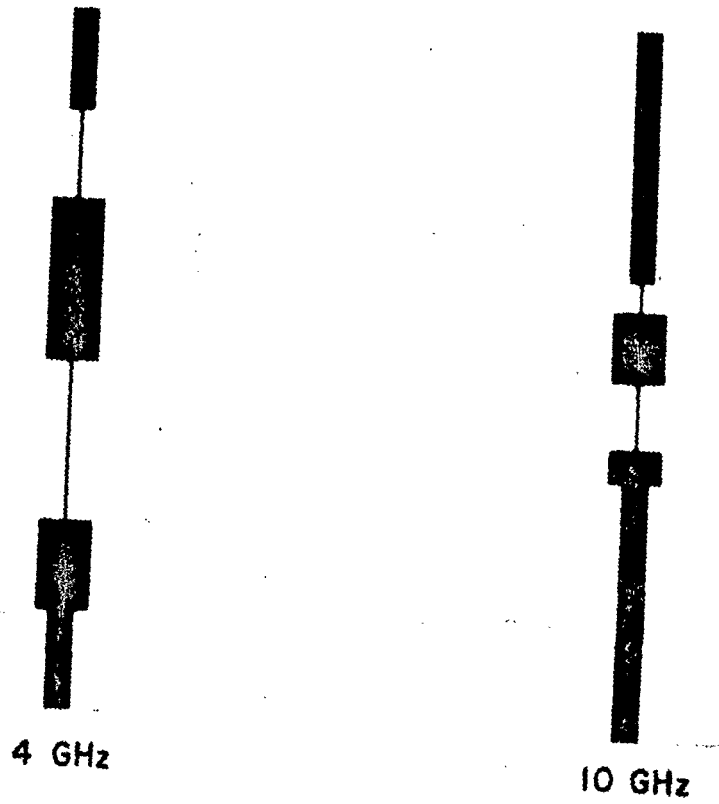


Figure 6. Lowpass Filter Mask Used for 4 GHz and 10 GHz Cutoff Frequency Design.

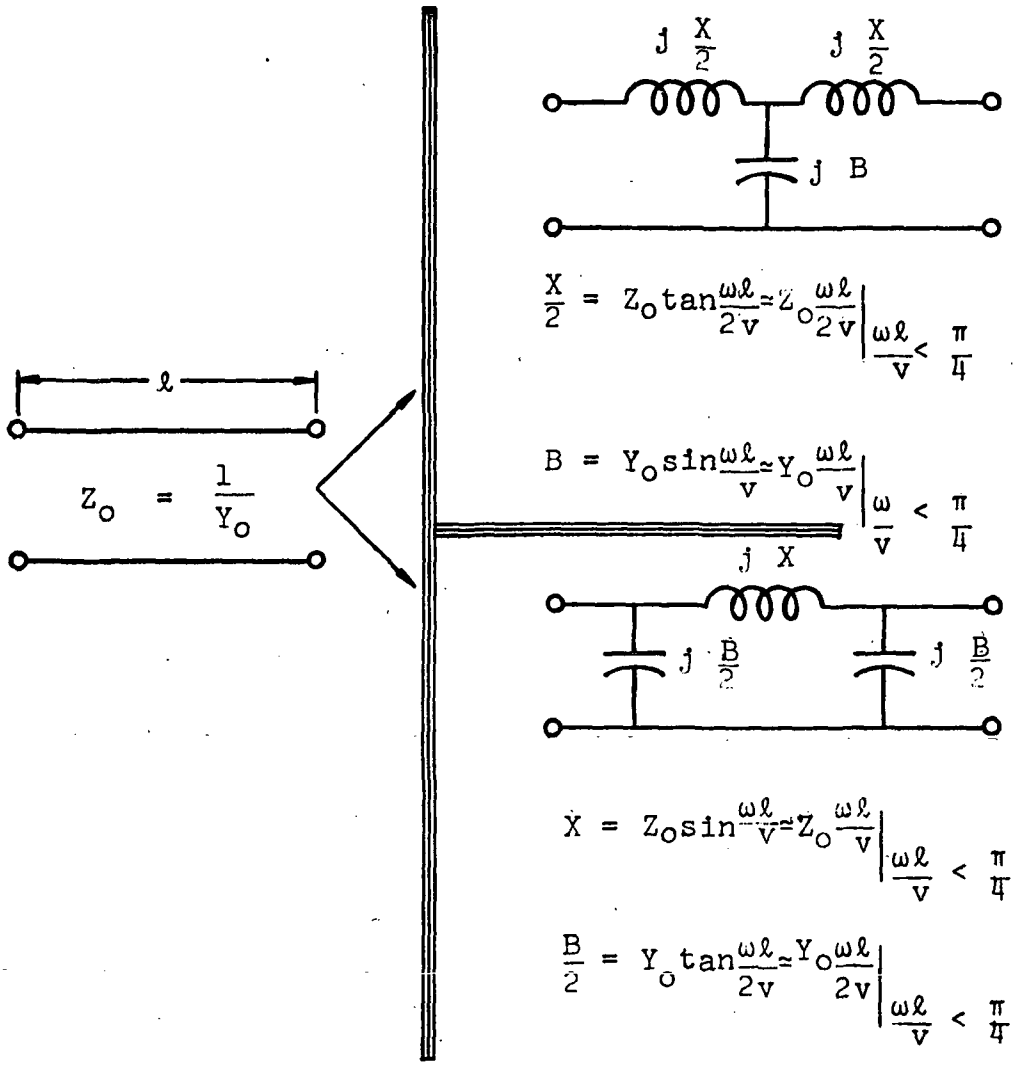


Figure 7. T and Π Equivalent Circuits for a Length of TEM Non-Dispersive Transmission Line.

$$\omega_1 L_i = Z_h \sin\left(\frac{\omega_1 \ell_i}{v_h}\right) + \frac{Z_\ell \ell_{i-1} \omega_1}{2v_\ell} + \frac{Z_\ell \ell_{i+1} \omega_1}{2v_\ell} \text{ ohms} \quad (2.20)$$

where

$Z_h, Z_\ell$ = characteristic impedance of the inductive and capacitive sections respectively.

$\omega_1$ = design radian frequency.

$L_i$ = inductance of the $i^{th}$ section.

$v_h, v_\ell$ = velocity of propagation in the inductive and capacitive sections respectively.

$\ell_i$ = physical length of the $i^{th}$ section.

Similarly, the capacitance of the low impedance section needs to be corrected by the fringing capacitances between the low and high impedance sections, and by the equivalent capacitance of the high impedance sections lumped at the ends of each section. The fringing capacitance is a function of the intrinsic capacitance of the elemental section in addition to the relative dielectric constant and strip width (23). The corrected capacitance elements can now be defined as:

$$\omega_1 C_i = \frac{Y_\ell \ell_i \omega_1}{v_\ell} + 2C_f \omega_1 + \frac{Y_h \ell_{i-1} \omega_1}{2v_h} + \frac{Y_h \ell_{i+1} \omega_1}{2v_h} \text{ mhos} \quad (2.21)$$

where

$C_i$ = capacitance of the $i^{th}$ section.

$Y_\ell, Y_h$ = admittance of the capacitive and inductive sections respectively.

$C_f$ = fringing capacitance.

In a typical design procedure, the inductance terms are taken directly from prototype values. These are used to compute initial capacitance values which are then used to get corrected inductance values. Repeated iterations are unnecessary since correction terms are truly second order.

In designing a lowpass filter a prototype design must first be chosen. Maximally flat and Tchebyscheff responses are well known (23) for filters with up to fifteen elements. Prototype responses are given in Reference (23) for elemental reactances normalized with respect to unit radian frequency and reactance, assuming series inductances and shunt capacitances. After pass and stop band responses have been determined from previous considerations, the required number of elements is determined from the above mentioned responses.

The normalized reactance must then be converted to realizable values dependent on both frequency and the transmission medium. For instance, a unity inductance is equivalent to $7.96 \times 10^{-10}$ henries for a 50Ω impedance at 10 GHz. Given the required inductance of the element, its length can then be computed as a function of impedance and velocity of propagation.

$$\ell = \frac{vL}{Z_o} \qquad (2.22)$$

where all quantities have been defined previously. A similar process can be carried out for the shunt capacitive elements.

An analysis was carried out for lowpass filters fabricated on microstrip. It is based on cascading several sections of transmission lines of various impedances and lengths. The input impedance is calculated at the end of each section and finally the entire device is represented as a frequency dependent input impedance.

$$\bar{Z}_{IN} = \frac{Z_{IN}}{Z_o} = \frac{Z_L + jZ_o \tan \beta\ell}{Z_o + jZ_L \tan \beta\ell} \tag{2.23}$$

$$= \frac{\text{Re } \bar{Z}_L \cos \beta\ell + j[\text{Im}\bar{Z}_L \cos\beta\ell + \sin \beta\ell]}{[\cos \beta\ell - \text{Im}\bar{Z}_L \sin \beta\ell] + j \text{ Re } \bar{Z}_L \sin \beta\ell} \tag{2.24}$$

where

$\bar{Z}_{IN}$ = normalized input impedance

$Z_o$ = characteristic impedance

$\beta\ell$ = $2\pi f \ell \sqrt{K_{eff}}$

$f$ = frequency

$\ell$ = length of the section

$K_{eff}$ = relative dielectric constant.

$\bar{Z}_L$ = $\text{Re } \bar{Z}_L + j\text{Im}\bar{Z}_L$ = normalized load impedance.

After rationalizing Equation (2.24), the following expressions result:

$$\text{Re } \bar{Z}_{IN} = \frac{\text{Re } Z_L}{[\cos \beta\ell - \text{Im}\bar{Z}_L \sin \beta\ell]^2 + [\text{Re } \bar{Z}_L \sin \beta\ell]^2} \tag{2.25}$$

$$\mathrm{Im}\bar{Z}_{IN} = \frac{\mathrm{Im}\bar{Z}_L \cos^2 \beta\ell + [(1-\mathrm{Im}\bar{Z}_L^2 - \mathrm{Re}\ \bar{Z}_L)\sin^2 \beta\ell]/2}{[\cos \beta\ell - \mathrm{Im}\bar{Z}_L \sin \beta\ell]^2 + [\mathrm{Re}\ \bar{Z}_L \sin \beta\ell]^2} \qquad (2.26)$$

The reflection coefficient $\Gamma$ can then be expressed in terms of the real and imaginary input impedances

$$\mathrm{Re}\Gamma = \frac{\mathrm{Re}\ \bar{Z}_{IN}^2 + \mathrm{Im}\ Z_{IN}^2 - 1}{(\mathrm{Re}\ \bar{Z}_{IN}+1)^2 + (\mathrm{Im}Z_{IN})^2} \qquad (2.27)$$

$$\mathrm{Im}\Gamma = \frac{2\mathrm{Im}\ \bar{Z}_{IN}}{(\mathrm{Re}\ \bar{Z}_{IN}+1)^2 + (\mathrm{Im}\bar{Z}_{IN})^2} \qquad (2.28)$$

The reflection coefficient then yields the insertion loss directly.

$$\text{Insertion loss (db)} = [-10 \log_{10}(1 - |\Gamma|^2] \qquad (2.29)$$

2.3.2 Results

Figure 8 shows both experimental results for a .01 db ripple four-element Tchebyscheff lowpass filter pictured in Figure 6 and the analysis based on the above calculations. In the analysis, terminations corresponding to a VSWR of 1.2:1 were used to simulate the degradation due to the OSM to microstrip transitions. Also shown in Figure 8 are the theoretical results of Equation (2.29).

Several things should be mentioned here about the correlation between experimental and theoretical results. Looking at Figure 8, it can be seen that the two curves, predicted and measured, appear to be offset in frequency. This is the result of omitting the correction factor mentioned earlier in the transmission line analysis of the

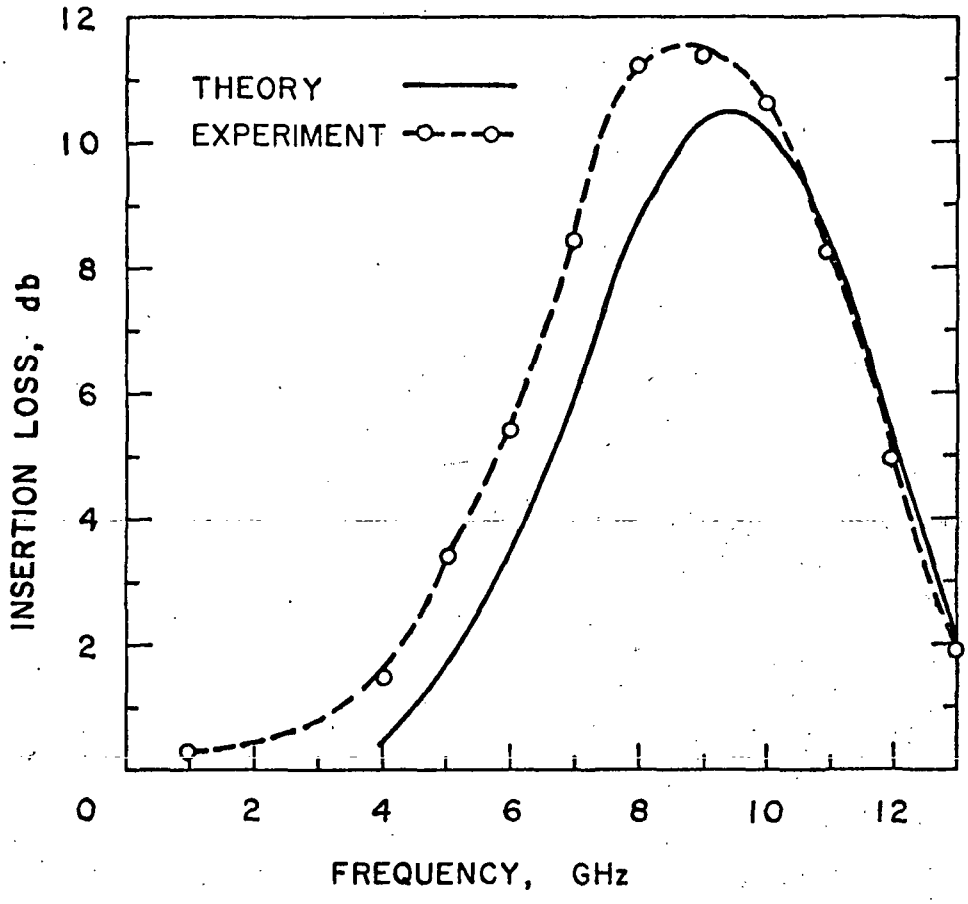


Figure 8. Lowpass Filter Insertion Loss vs. Frequency for a 4 GHz Cutoff, 4 Element Filter.

filter. The net result of these corrections would be to lengthen the filter and therefore to lower the frequency response, thus more nearly bringing the two curves into coincidence.

Furthermore, it is seen that the predicted curve has both higher Q and lower maximum insertion loss. It is believed that this is the result of using a non-dispersive loss free approximation in the transmission line analysis.

Probably the most striking feature of the predicted and measured responses is the spurious pass-band at 13 GHz. This is the result of not using a required impedance transformer for a lowpass filter with an even number of elements (23). The lowpass filter used in the mixer circuit has six elements and is described in Chapter 3 where the first circuit and its performance are given.

## 2.4 TRAVELING-WAVE DIRECTIONAL FILTER

The traveling wave directional filter can be defined (24) as a four-port, constant resistance network with the following characteristics. With power incident on any one port, the remaining three ports remain matched so that the input reflection coefficient is zero, the transfer function between the input port and a second port is band-pass, while the transfer function between the input port and a third port is band stop, and the fourth port is isolated. These ideal transmission characteristics are summarized in Figure 9.

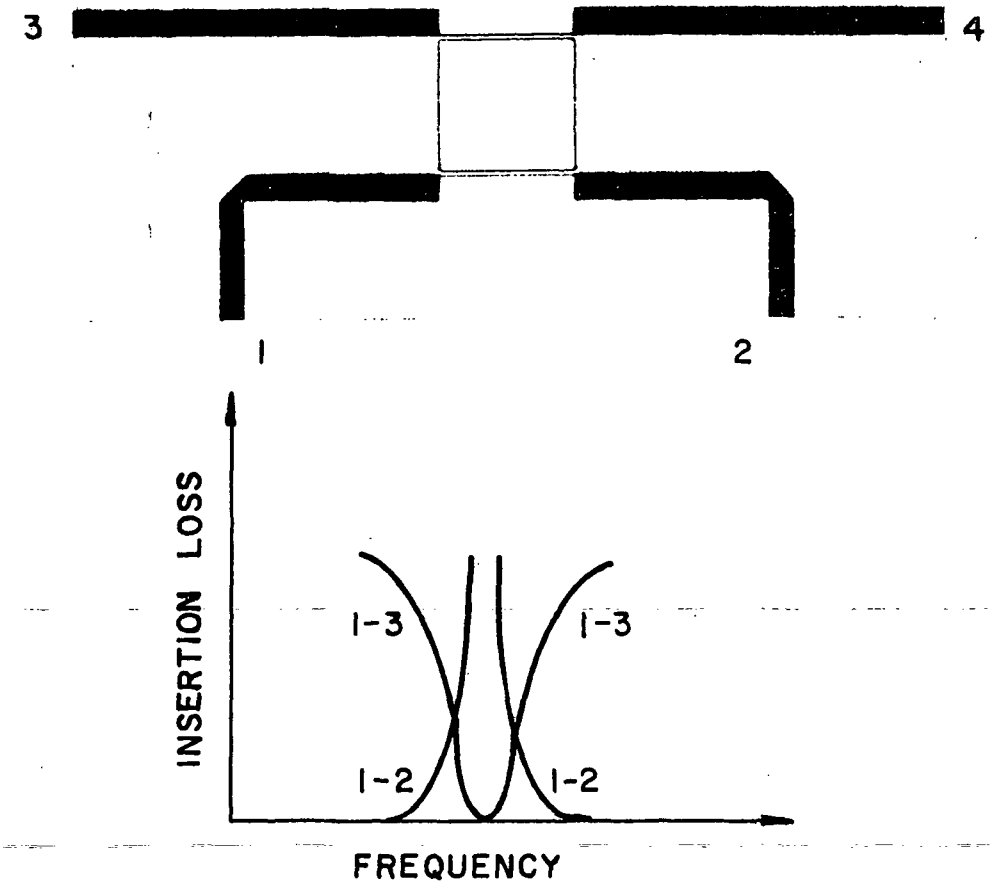


Figure 9. Microstrip Traveling-Wave Filter Mask and Ideal Response Characteristics.

2.4.1 Design and Analysis

The traveling wave directional filter was first reported by Coale(25). One of the distinguishing characteristics of the resonant loop is that resonant energy is in the form of traveling waves as opposed to standing wave resonances as would be found in a cavity resonator. Also, if the coupling coefficient of the directional couplers are chosen properly, 100 per cent of the input to the first coupler can be extracted by the second coupler (24). With additional loops between the two couplers, the desired response can be effected.

An attempt was made to analyze the traveling-wave filter by constructing the 4 x 4 scattering matrix of the device and then cascading it with the input voltage column matrix in a fashion exactly analogous to that pursued for the directional coupler analysis in Section 2.2.1 of this chapter. This attempt did not yield satisfactory results. It is believed that the major source of error is the fact that the scattering parameters used rely on reference plane locations inconsistent for the given device.

Standley (24) has carried out an analysis that reduces the four-port problem to that of two equivalent two-port problems. The reduction is based on applying, alternately, symmetrical and anti-symmetrical excitations to two of the four ports. The response characteristics are then found

by superposition of the transfer and reflection coefficients for the two cases.

In the analysis of the ideal case, it is assumed that all transmission lines have the same characteristic impedance, there are no discontinuities internal to the loop and the device is lossless. This result is then extended to the case where the impedance of the sections connecting the coupled lines are not equal to the characteristic impedance of the balance of the system (26). The structure is now as pictured in Figure 10.

Carrying out Standley's (26) symmetric, anti-symmetric analysis for this structure, the following transfer and reflection coefficients result, where the subscript S refers to symmetric analysis and A refers to the anti-symmetric excitation:

$$
\begin{aligned}
T_S = 2\Big\{ & [2(\cosh 2\alpha \cos \beta_I + \frac{\sin \beta_I \sinh 2\alpha}{2} \\
& \cdot (\frac{Z_o}{Z_I} \cot \theta - \frac{Z_I}{Z_o} \tan \theta))] \\
& + j[\sin \beta_I ((\frac{Z_o}{Z_I} + \frac{Z_I}{Z_o}) \cosh^2 \alpha - \sinh^2 \alpha \\
& \cdot (\frac{Z_I}{Z_o} \tan^2 \theta + \frac{Z_o}{Z_I} \cot^2 \theta)) \\
& + \cos \beta_I \sinh 2\alpha (\tan \theta - \cot \theta)] \Big\}^{-1}
\end{aligned}
\qquad (2.30)
$$

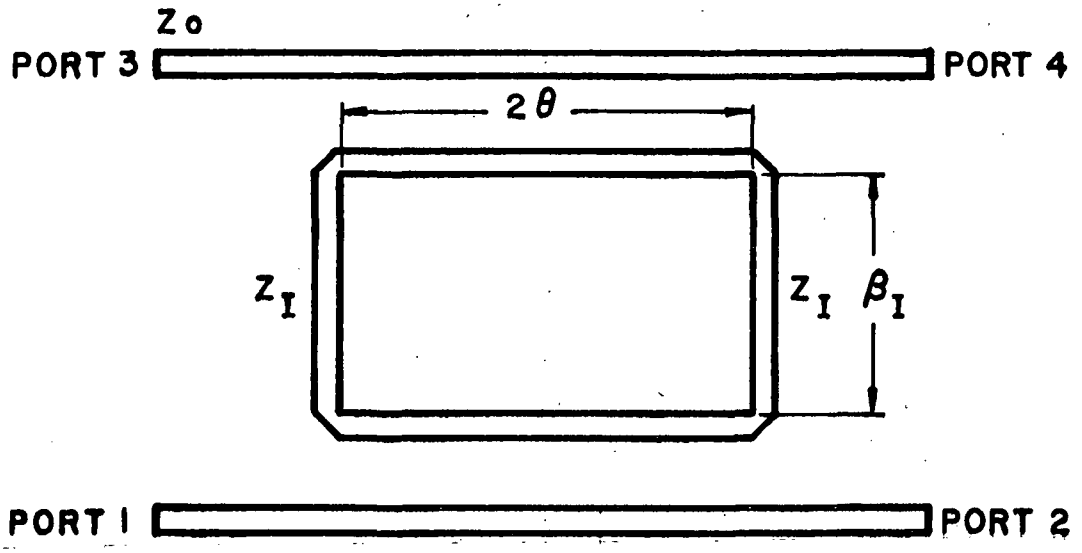


Figure 10. Directional Filter with Non-Uniform Impedance Resonant Loop.

$$T_A = 2\Big\{[2(\cosh 2\alpha \cos \beta_I + \frac{\sin \beta_I \sinh 2\alpha}{2} \cdot (\frac{Z_I}{Z_o} \cot \theta - \frac{Z_o}{Z_I} \tan \theta))] + j[\sin \beta_I((\frac{Z_o}{Z_I} + \frac{Z_I}{Z_o}) \cosh^2\alpha - \sinh^2\alpha \cdot (\frac{Z_I}{Z_o} \cot^2 \theta + \frac{Z_o}{Z_I} \tan^2 \theta)) + \cos \beta_I \sinh 2\alpha(\tan \theta - \cot \theta)]\Big\}^{-1} \quad (2.31)$$

$$\Gamma_S = -j \frac{T_S}{2}\Big\{\sin \beta_I[(\frac{Z_I}{Z_o} - \frac{Z_o}{Z_I}) \cosh^2 \alpha - \sinh^2 \alpha \cdot (\frac{Z_o}{Z_I} \cot^2 \theta - \frac{Z_I}{Z_o} \tan^2 \theta)] - \cos \beta_I \sinh 2\alpha(\cot \theta + \tan \theta)\Big\} \quad (2.32)$$

$$\Gamma_A = j \frac{T_A}{2}\Big\{\sin \beta_I[(\frac{Z_I}{Z_o} - \frac{Z_o}{Z_I}) \cosh^2 \alpha + \sinh^2 \alpha \cdot (\frac{Z_I}{Z_o} \cot^2 \theta - \frac{Z_o}{Z_I} \tan^2 \theta)] + \cos \beta_I \sinh 2\alpha(\cot \theta + \tan \theta)\Big\} \quad (2.33)$$

where

$\cosh \alpha = \frac{Z_{oe} + Z_{oo}}{Z_{oe} - Z_{oo}}$ and all other symbols are as in Figure 10.

Equation (2.30) through Equation (2.33) can then be used to determine the scattering parameters for the four by four matrix describing the traveling-wave filter. Standley (24) has determined that there are only four unique elements:

$$[S] = \begin{bmatrix} S_{11} & S_{12} & S_{13} & S_{14} \\ S_{12} & S_{11} & S_{14} & S_{13} \\ S_{13} & S_{14} & S_{11} & S_{12} \\ S_{14} & S_{13} & S_{12} & S_{11} \end{bmatrix} \tag{2.34}$$

In terms of the transfer and reflection coefficients defined above, the scattering parameters are:

$$S_{11} = \frac{\Gamma_S + \Gamma_A}{2} \tag{2.35}$$

$$S_{12} = \frac{\Gamma_S - \Gamma_A}{2} \tag{2.36}$$

$$S_{13} = \frac{T_S + T_A}{2} \tag{2.37}$$

$$S_{14} = \frac{T_S - T_A}{2} \tag{2.38}$$

The scattering parameters above are sufficient to determine the fundamental response and general nature of the traveling-wave directional filter.

In the actual design procedure, the resonant ring is a full wavelength in circumference with each side a quarter-wavelength long. One of the first corrections to this seemingly simple design task is to include the effects of the mitered corners in microstrip. These effectively shorten the sections of the ring that interact with the two coupled sections of transmission line.

Another consideration is the degree of coupling for the input and output coupling sections. It would appear that tight coupling would be required in order to achieve

low insertion loss across the traveling-wave resonant ring, a specification for its implementation as a diplexer. From data available in the literature (18,23) it can be seen that this is accomplished by going to high impedance microstrip coupled transmission sections. Since the balance of our system is 50Ω, quarterwave impedance transformers were first used to match the high impedance coupling sections to each port. This effort proved to be unsatisfactory. Acceptable results were obtained after removing the transformer sections.

2.4.2 Results

The analysis for this filter incorporates the formulae stated above for the four independent scattering parameters. Experimental and predicted results can be found in Figures 11 through 13.

A number of observations should be made at this point. First, reasonable results were found for the two coupled ports but not for the "isolated" response. It is believed that this is due to the fact that the characterization of the device was found to be dependent mainly on the coupling coefficient and the degree of internal mismatch for the resonant ring. However, external port mismatches were not accounted for in this analysis. Standley's (26) results also predict very poor isolation for the device contrary to experimental evidence shown in Figure 13. The error is on the order of 10db.

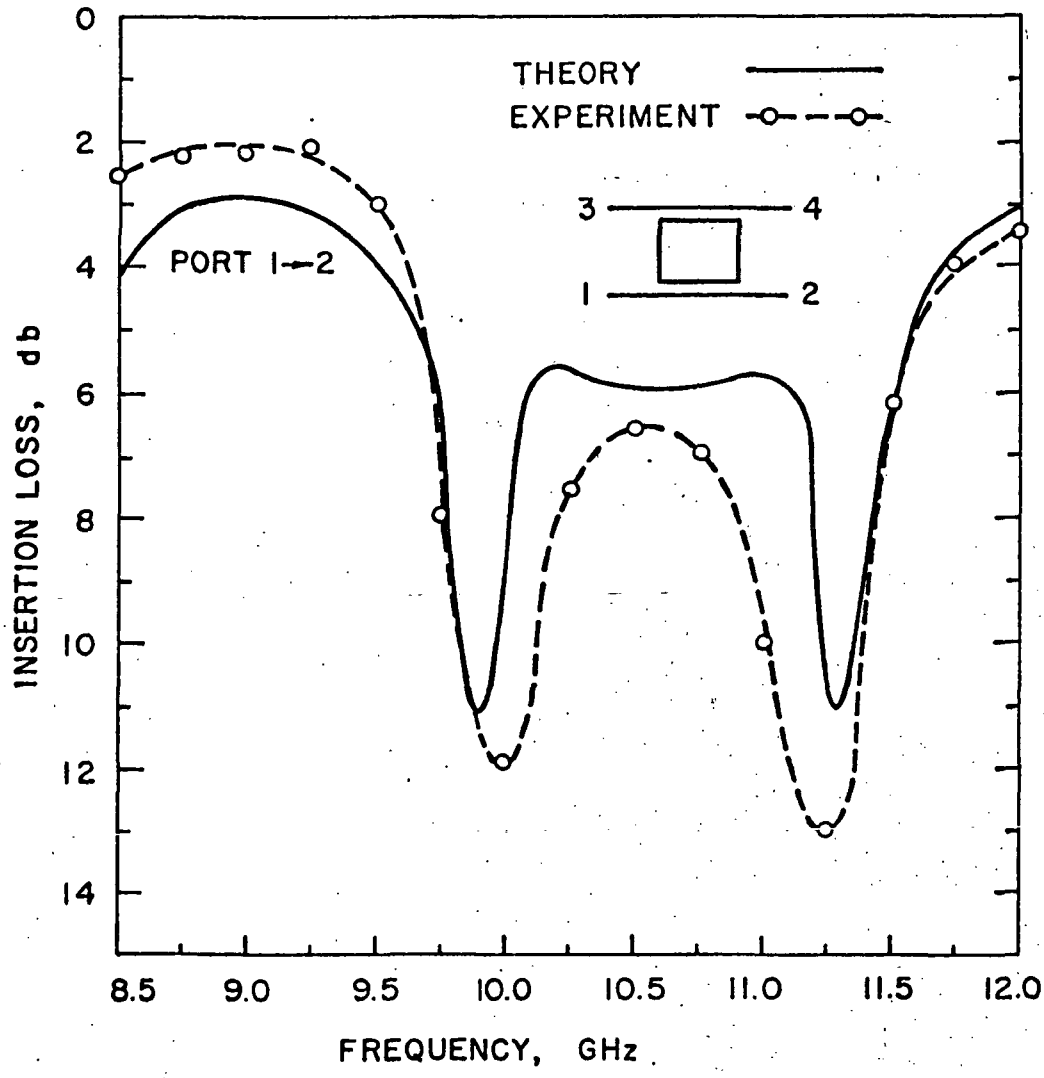


Figure 11. Traveling-Wave Directional Filter Port 1→2 Insertion Loss vs. Frequency.

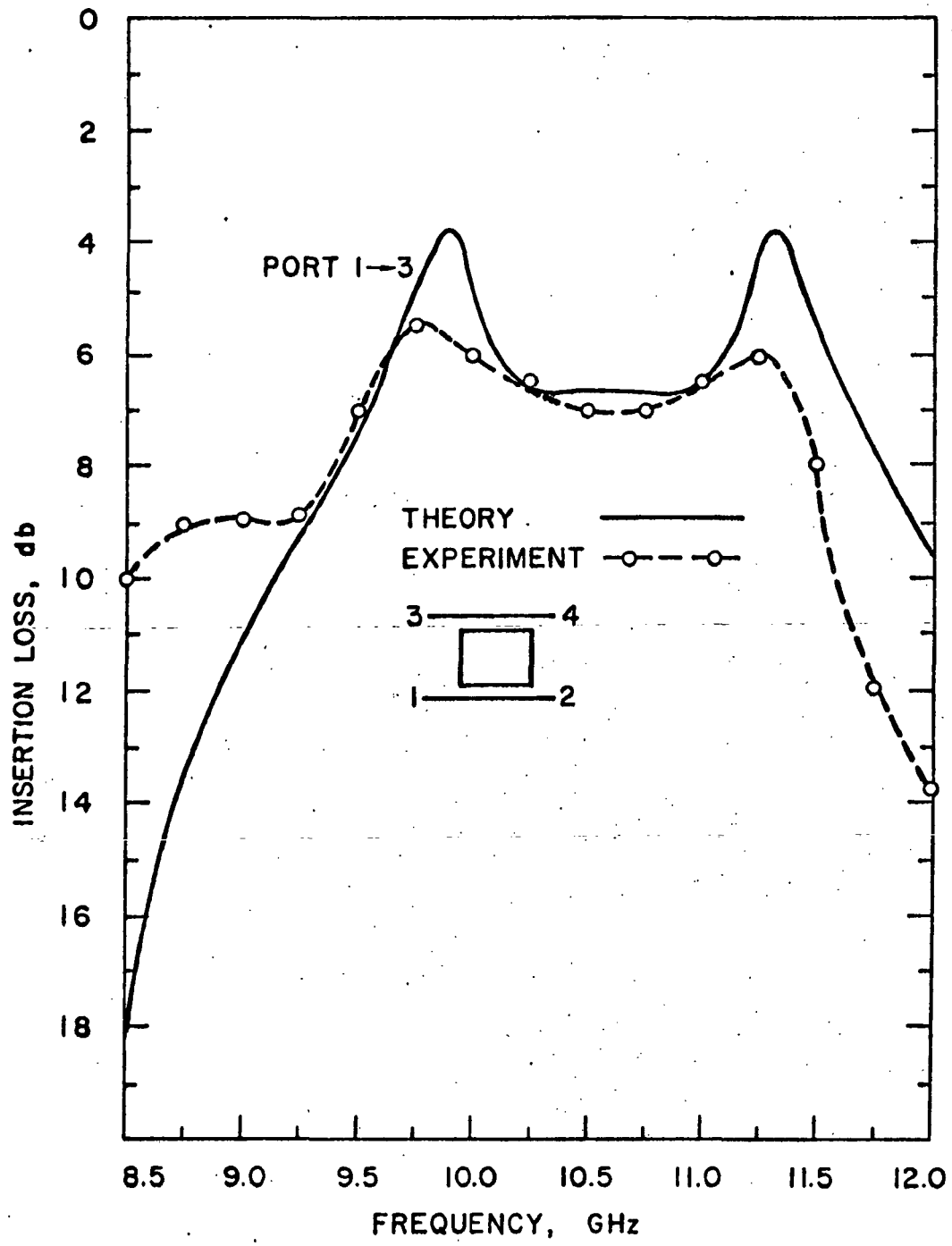


Figure 12. Traveling-Wave Directional Filter Port 1→3 Insertion Loss vs. Frequency.

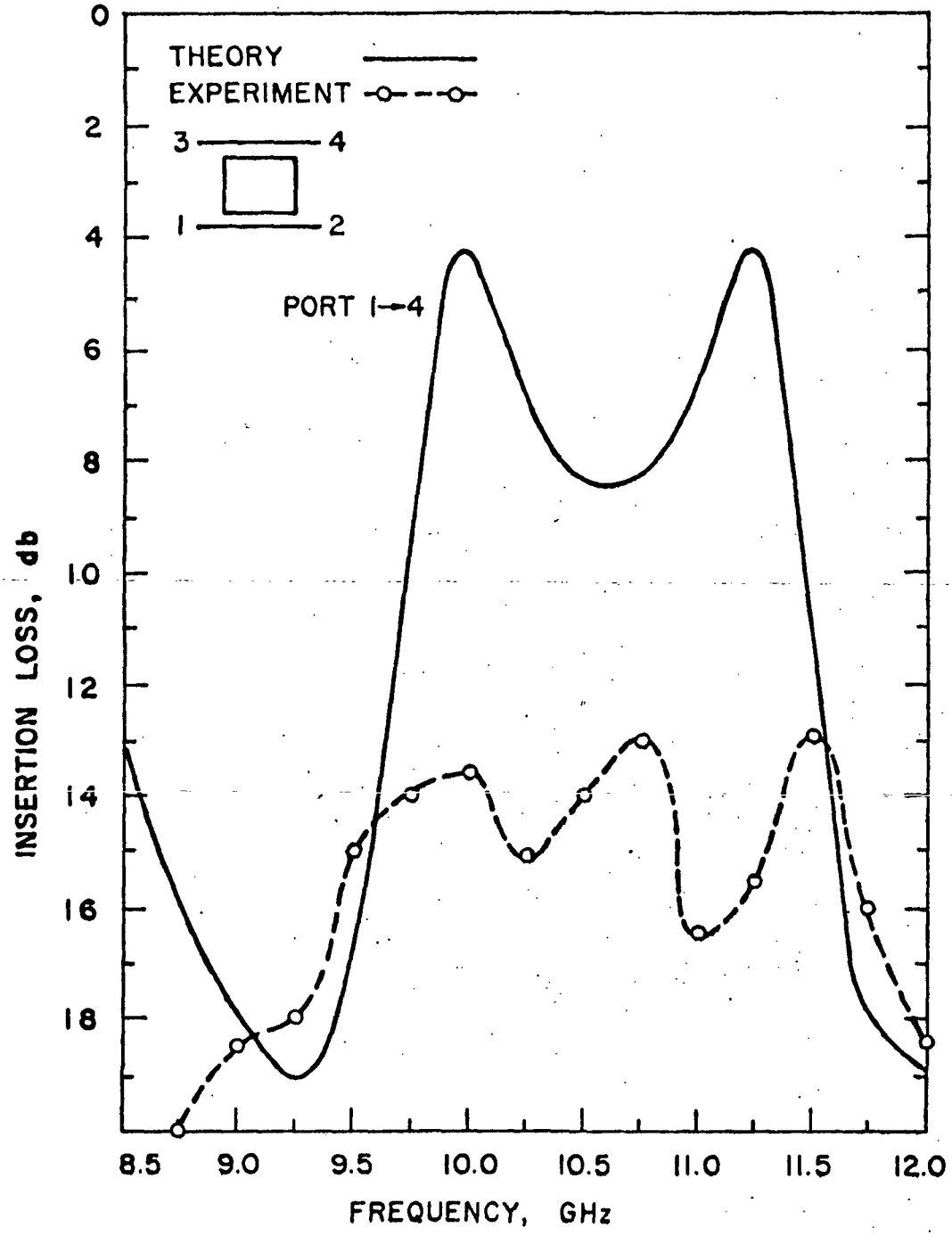


Figure 13. Traveling-Wave Directional Filter Isolated Port 1→4 Insertion Loss vs. Frequency.

The above discussion, however, should not overshadow the basic success of Standley's analysis in predicting the overall behavior of the device. The internal mismatch parameter taken alone does allow one to predict the magnitude and location in frequency of the double peak response for ports 1→2 and 1→3. This double response was not predicted or accounted for by other workers (23,25).

If further work is to be done on this device it is felt that the analysis should be revised to include the effects of external port mismatch. With this modification, a model of sufficient accuracy should result precluding the need for numerous experimental iterations normally required when optimizing this device.

## 2.5 QUARTER-WAVE STOP-BAND FILTER

Also considered was a rejection or band-stop filter. The specific type, pictured in Figure 14, has been described in the literature (14,27) and has been used for the same purpose, namely image and sum enhancement techniques.

This structure was proposed by Jones and Bolljahn (28) and is pictured in Figure 15. In that figure,

$$Z_{I_1} = \frac{2Z_{oe}Z_{oo}\cos\theta}{[-(Z_{oe} - Z_{oo})^2 + (Z_{oe} + Z_{oo})^2\cos^2\theta]^{1/2}} \quad (2.39)$$

$$Z_{I_2} = \frac{Z_{oe}Z_{oo}}{Z_{I_1}} \quad (2.40)$$

$$\cos\theta_{c1} = -\cos\theta_{c2} = \left[\frac{\frac{Z_{oe}}{Z_{oo}} - 1}{\frac{Z_{oe}}{Z_{oo}} + 1}\right] \quad (2.41)$$

where $Z_{oe}$, $Z_{oo}$ are the even and odd mode impedances respectively.

$\theta$ = electrical length of the coupled section.

Again referring to Figure 15, it can be seen that the structure can be used in a low-pass, stop- or pass-band mode depending on the design frequency and range of use.

Our application required the stop band mode and, therefore, the coupled section was designed to be $\pi/2$ long at the desired frequency. The design goal was to achieve a minimal insertion loss in the pass band region while retaining a reasonable stop-band capability at the

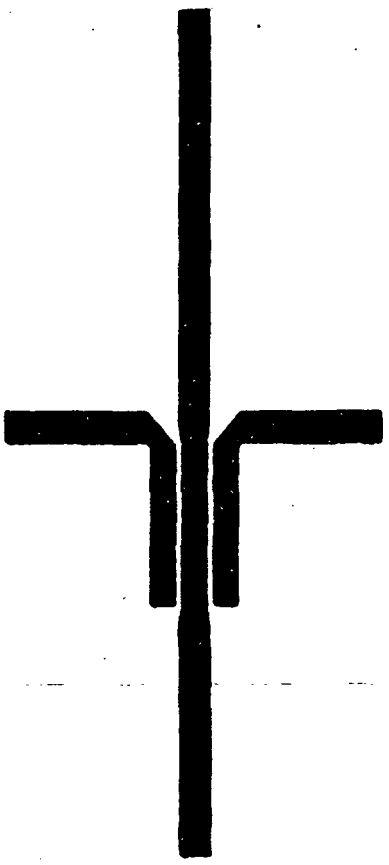

50Ω FILTER

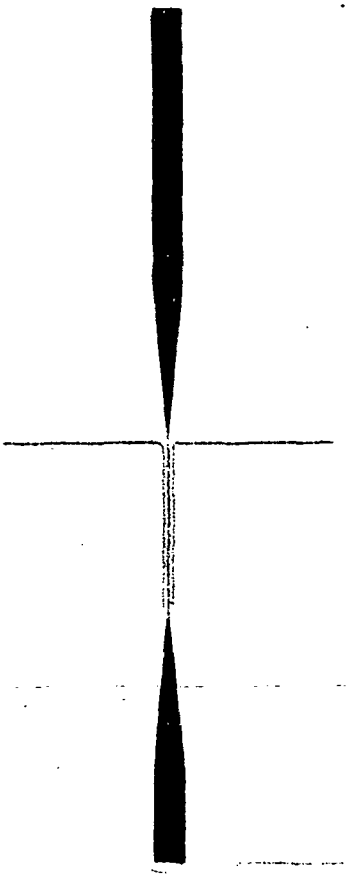

HIGH IMPEDANCE FILTER
WITH IMPEDANCE MATCHING
TRANSFORMERS

Figure 14. Rejection Filters with and without Impedance Matching Transformers.

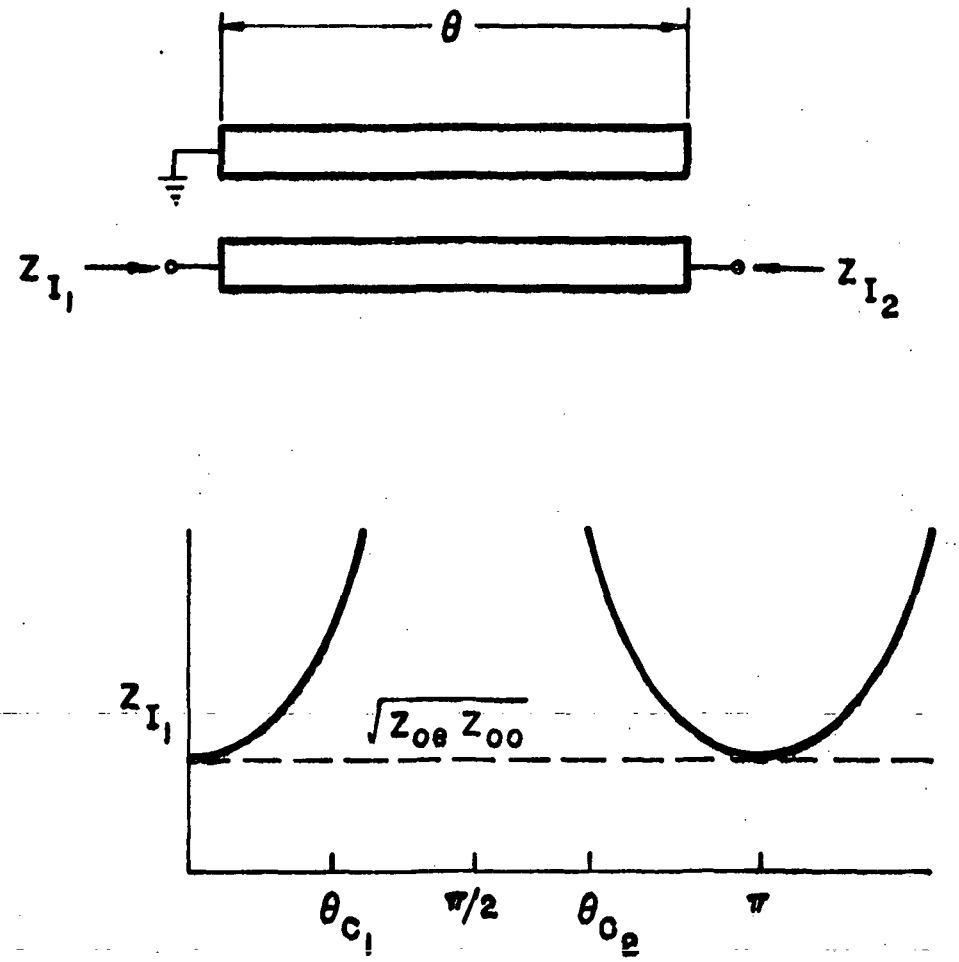


Figure 15. A Coupled Microstrip Transmission Line Segment and Its Response.

design frequency. It was thought that this could best be achieved with high impedance lines and therefore tight coupling sections matched to 50Ω input and output by quarter-wave impedance transformers were investigated first. This approach resulted in an unsatisfactory filter response.

A uniform 50Ω structure was then fabricated. Its experimental insertion loss characteristic is shown in Figure 16. It exhibits a high insertion loss of 24db at the design frequency with a 3db bandwidth of 200MHz. With further iteration in the design, it is felt that the necessary 500MHz bandwidth could be achieved.

Looking at Figure 16, it is seen that the residual passband insertion loss is on the order of 2db. The total length of the test filter was one inch, which accounts for 0.8 db of insertion loss due to dissipative dielectric loss. For integration in the final mixer circuit, the dissipative loss due to the filter would be negligible since the signal path length would not need to be increased. The additional one db of loss is due to a VSWR of 2:1 to 2.6:1 in the passband region of the filter.

The proposed use of this filter, i.e., image and sum enhancement, would each produce improvements in the overall noise performance of under one db. Therefore, for this filter to be of use, further work would have to be done to improve the passband VSWR.

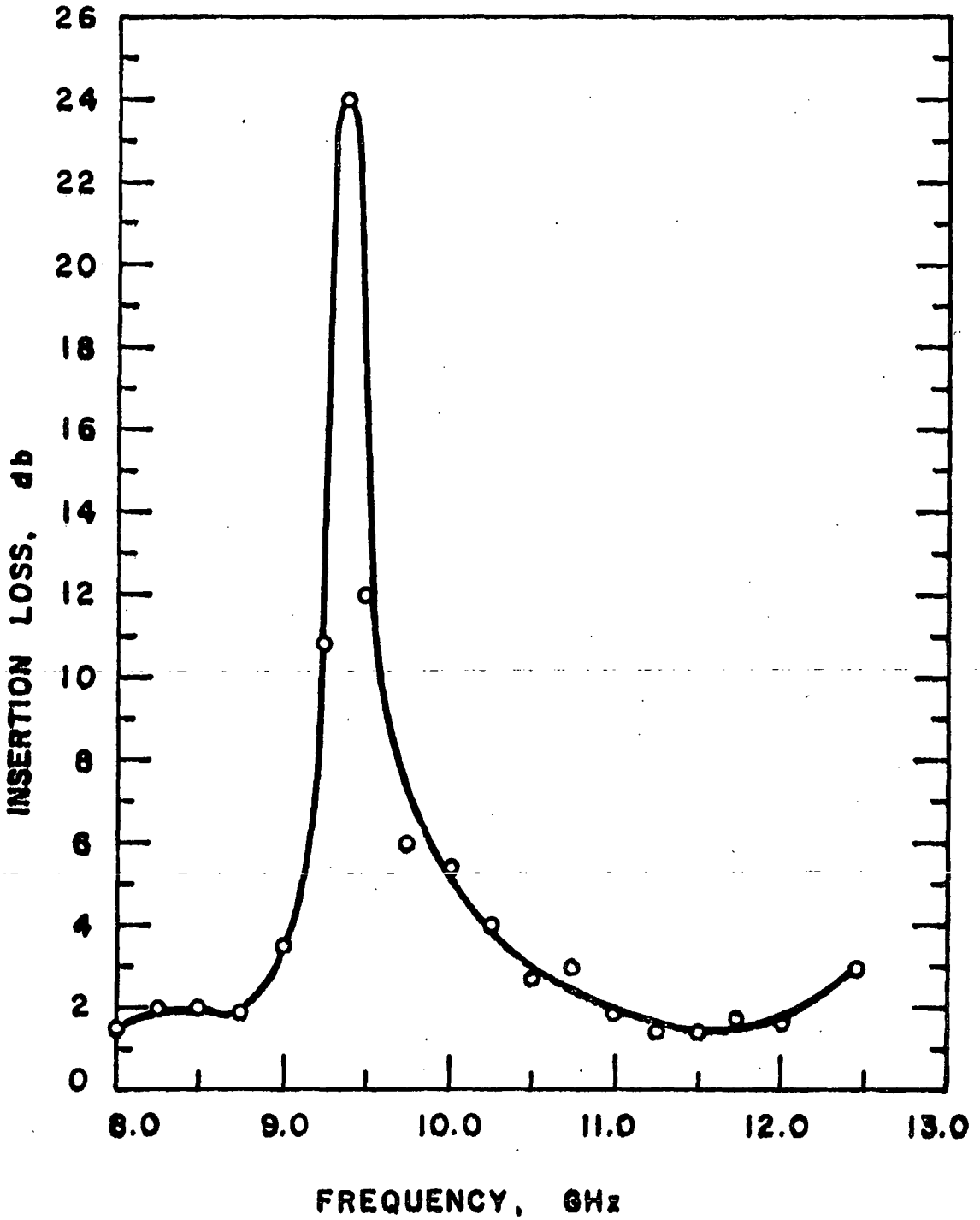


Figure 16. Quarter-Wave Stop-Band Filter Insertion Loss vs. Frequency.

# 3. MIXER DESIGN

## 3.1 GENERAL DESIGN CONSIDERATIONS

In a previous systems analysis (1) carried out at Washington University, justification for the overall design of the frontend was given. It will be highlighted here along with a description of the final hardware implementation.

One of the significant features of the design is the fact that the mixer is single ended (single diode). This configuration was chosen because the modulation scheme for the proposed transmit-receiver system is wideband FM. Therefore, no benefits accrue due to LO AM noise suppression afforded by a balanced circuit. Since wide bandwidth can be achieved with single-ended mixers (see Reference 14), simplicity of design and cost-effectiveness also suggest this approach.

Another feature of the design is the use of field replaceable diodes. It is felt that this type of receiver would experience less down-time due to diode burnout, since a packaged diode could easily be replaced without trained personnel and expensive equipment. This is in sharp contrast to the replacement of beam lead or chip diodes. It is felt also that it is cheaper for a head end operator to stock spare diodes than an entire front end. Finally, the use of packaged diodes precludes the need for hermetic sealing of the entire front end assembly.

The schematic diagram of the front end is shown in Figure 17. The signal and local oscillator frequencies are introduced to the mixer through waveguide inputs. The signal input was chosen to be waveguide so as to be compatible with either a receive antenna or a waveguide amplifier, should one be found necessary to reduce the overall system noise figure. The waveguide prevents IF leakage from the signal port by virtue of its inherent highpass properties. The local oscillator port is also waveguide since this choice allows the use of a high Q imbedding network for a Gunn effect diode necessary for stable, low noise output (8).

Microstrip was chosen as the medium in which to fabricate the diplexer and associated filters. This choice allows package size reduction as well as volume cost reduction after the circuit has been finalized.

It was decided that the mixer crystal would be operated without an external DC bias. As is the case with other mixers reported in the literature (14,15) a self-biased diode was chosen since increased LO drive levels to achieve low conversion loss seemed more desirable than an additional DC power supply. More accurately, the crystal was operated at DC ground by providing a DC return from the signal path to the down-converter housing. It is not expected that a variable DC bias would have resulted in an improved noise figure since although the crystal IF impedance can be lowered

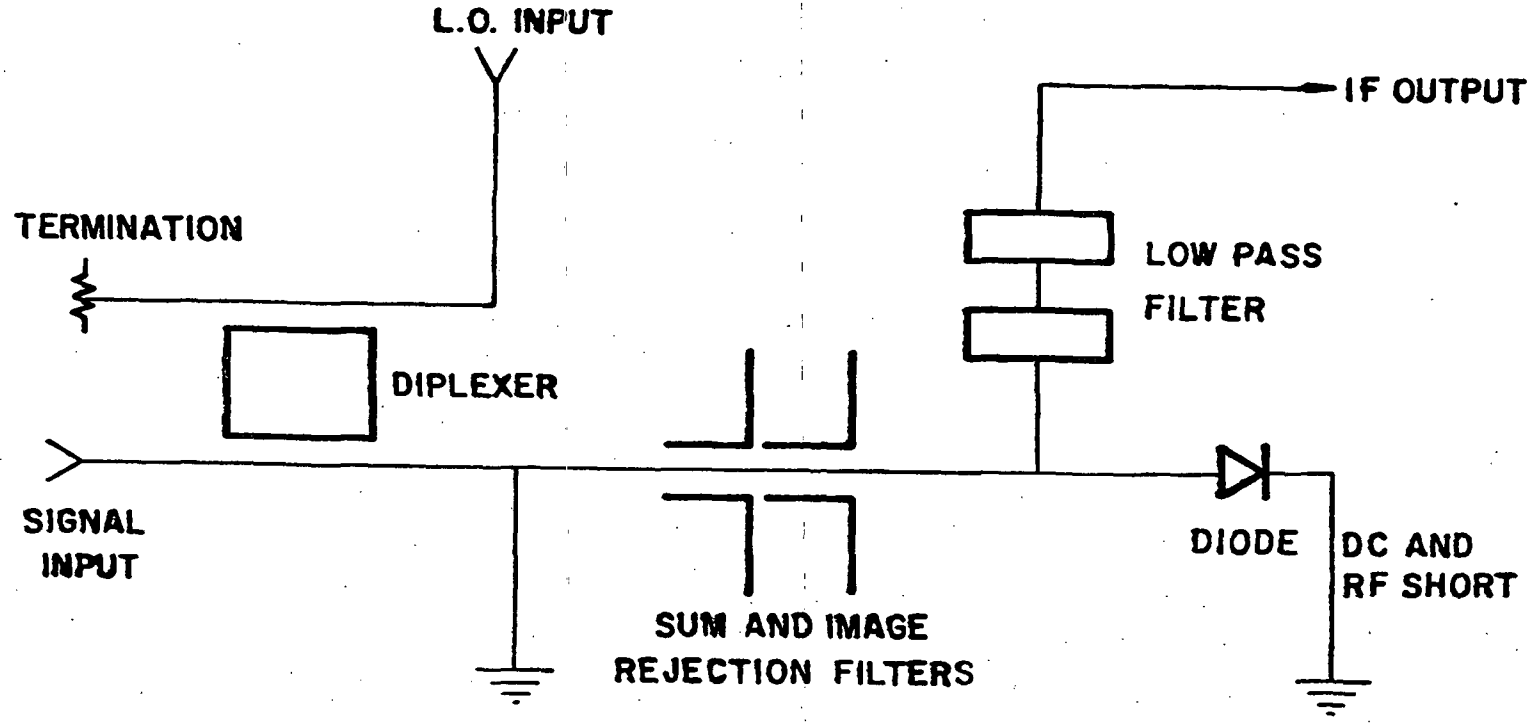


Figure 17. Schematic of Mixer Circuit First Considered.

by providing a better match, the noise ratio increases with DC bias.

One of the first stages in the development of the frontend was the design of a 50Ω coaxial crystal mount to be used with both point contact and Schottky Barrier Diodes in standard ceramic cartridge packages. The low frequency (30MHz) IF was extracted through a BNC bulkhead mount. DC ground was achieved with a fine wire leading from the center conductor to the outer conductor. RF bypassing was accomplished by using 0.005in mylar tape on a washer in pressure contact with one terminal of the diode. This proved to be inadequate since changes in the pressure affected both the input match and its ability to bypass the RF. It was found that with additional microwave impedance matching (tuning screws) a 2:1 VSWR could be obtained over the band 10.4GHz to 12.4GHz.

The final down-converter housing is pictured in Figure 18. The overall dimensions are 4 3/4 in x 3 5/8 in x 1 1/2 in. Waveguide inputs were fabricated by milling "U" shaped troughs in the aluminum block and then bolting cover plates over these slots. Rectangular waveguide to coaxial-waveguide to microstrip transitions were fabricated using 0.050in brass brazing stock as the center conductor. The end protruding into the waveguide uses a "doorknob" structure as an antenna. The center section has a teflon sheath for mechanical reasons and to provide a 50Ω coaxial

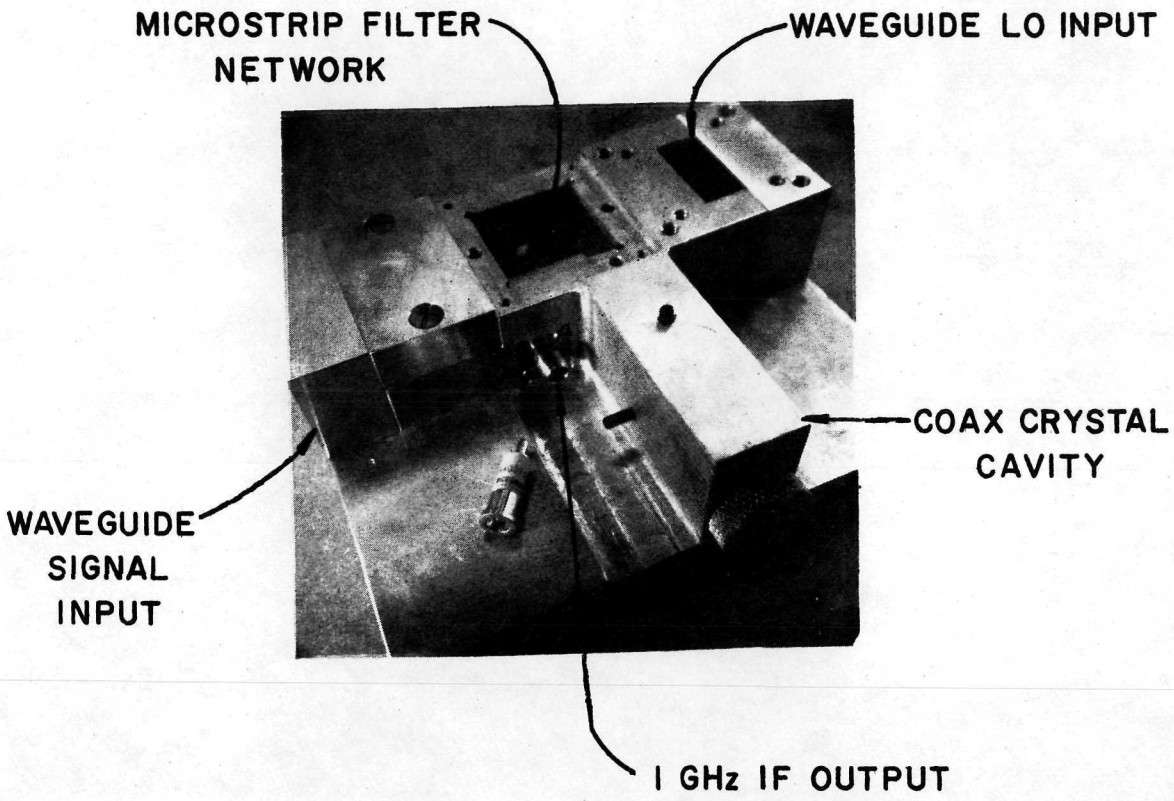


Figure 18. Down-Converter Package.

line. Finally, the center conductor tapers to a "half-round" to provide a transition to microstrip. The transitions exhibited a return loss of better than 18db (VSWR = 1.3) over the band 11.3GHz to 12.4GHz. The insertion loss of each transition is approximately 0.25db.

The 50Ω coaxial mount for the mixer diode was modified in the final package. The end of the cavity is a metal plug that provides both an RF short and part of the path necessary to provide a DC short to the diode. The rest of the DC return path is traced through the microstrip circuit to the housing. The IF is reflected from the RF short and taken from the mixer through a lowpass filter fabricated on the microstrip board.

The down-converter was designed to operate with several types of mixer crystals. For developmental purposes a cartridge type silicon point contact diode, Microwave Associates IN23E was chosen. Its advertised performance in the high x-band is: Maximum Noise Figure, 7.5db; Maximum Conversion Loss, 5.0db; Maximum VSWR, 1.3:1.

A relatively low cost silicon Schottky Barrier mixer diode was also used. The ceramic cartridge type was the MA-4007IE with manufacturer's specs given as: Maximum Noise Figure, 7.5db; Conversion Loss, 6.0db; Maximum VSWR, 1.5:1. Finally, the coaxial cavity was modified to accomodate a GaAs Schottky Barrier Diode. Specifications for the Mitsubishi pill-prong diode were not available with the

exception of the Noise Ratio which was assumed to be unity. This is reasonable for the given device (see Reference 15). The i-v characteristic for the Mitsubishi diode is given in Figure 19. From the part of the characteristic curve pictured in Figure 19, the diode appears to have an ideal exponential trace. To reduce the risk of diode burnout, the forward current was kept minimal. However, if the forward current is increased further, the diode conductance reaches a maximum level equal to the inverse of the spreading resistance (17). This, in turn, limits optimum conversion loss vs. LO drive as can be seen in Figure 23. Performance of the mixer with the crystals given above is given in Chapter 4.

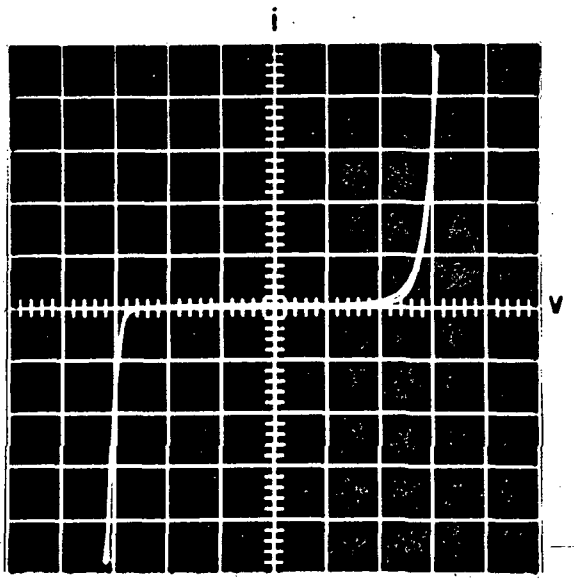


FORWARD UNITS: 0.2 v/cm , 0.2 ma/cm
REVERSE UNITS: 5 v/cm , 0.2 ma/cm

Figure 19. I-V Characteristic for Mitsubishi GaAs Schottky Barrier Diode.

## 3.2 MICROSTRIP CIRCUIT CONFIGURATIONS

In Section 3.1, an attempt was made to justify the choices made in the general design of the mixer. In this section, two specific microstrip transmission line circuits will be examined. The first is the one that we wanted to use and the second the one actually incorporated in the final down-converter.

The circuit originally considered is shown in Figure 17. The traveling-wave directional filter discussed in Section 2.4 presents itself as a very good choice for diplexing the the signal and local oscillator frequencies. The use of this filter as a diplexer has been mentioned in the literature previously (14). It is limited, however, to mixers with very high IF's on the order of 1GHz. The resonant ring is designed to be one wavelength at the LO frequency. This allows the LO to pass across the ring and onto the signal transmission line with minimal loss. Also, the signal frequency passes the resonant ring with minimum attenuation if it is of sufficiently higher or lower frequency. A 1GHz IF presents such a choice. The characteristics of this device, both experimental and predicted, are given in Section 2.4.

The diode and its mount are described in Section 3.1. After the signal and local oscillator are introduced to the diode, the IF is reflected from the coaxial short. The lowpass filter is located at a point of minimum insertion

loss with the aid of an IF bypass network that insures minimal loss for the signal path.

Finally, consider the image and sum frequency enhancement filters. These filters allow energy that would normally be lost to be reflected back into the diodes to be remixed to the intermediate frequency and extracted through the lowpass filter at the IF port. The various IF components are:

$$\omega_{IF} = \begin{bmatrix} \omega_S - \omega_{LO} \\ \omega_{LO} - \omega_I \\ \omega_\Sigma - 2\omega_{LO} \end{bmatrix} = \text{intermediate frequency} \qquad (3.1)$$

$\omega_S$ = $2\pi f_S$, signal radian frequency

$\omega_{LO}$ = local oscillator frequency

$\omega_I$ = $2\omega_{LO} - \omega_S$ = image frequency

$\omega_\Sigma$ = $\omega_{LO} + \omega_S$ = sum frequency

One of the basic questions involved in the use of rejection or enhancement filters is their placement with respect to the diode. This has been accomplished in the past (29) by experimentally varying the position of filters and noting the optimum performance, either conversion loss or noise figure. The other basic question in designing a mixer is to decide to reflect the image and sum frequencies with an open or short circuit. Although an open-circuited image results in a minimum noise figure, a short-circuited image results in a lower IF matching resistance (29). This

lower IF resistance reduces the need for narrow band matching circuits. Therefore, a wideband mixer can best be achieved with a short-circuited image (29).

It was decided, however, that the above circuit would not result in the best overall performance for the down-converter for the following reasons. First, referring to Figure 11, the minimum insertion loss for the signal through the traveling-wave directional filter is seen to be around 2db. This is not acceptable since any loss in advance of the mixer adds directly into the overall noise figure. Thus, 2db of loss at this point would make a low loss device impossible. Secondly, referring to Figure 16, it can be seen that the insertion loss of a rejection filter off the design frequency is about 2db. A loss of this magnitude cannot be tolerated since enhancement techniques can at best improve the overall noise figure by less than one db (14).

The circuit actually used is shown schematically in Figure 20 and a picture of the actual microstrip mask is shown in Figure 21. The reason for using a directional coupler to multiplex the signal and LO in place of the traveling wave directional filter is because of the lower insertion loss presented to the signal frequencies. The port designated AFC output was not so used in this experiment. Its purpose is to provide a sample of the LO if Automatic Frequency Control must be implemented. The final circuit does not incorporate either image or sum enhancement

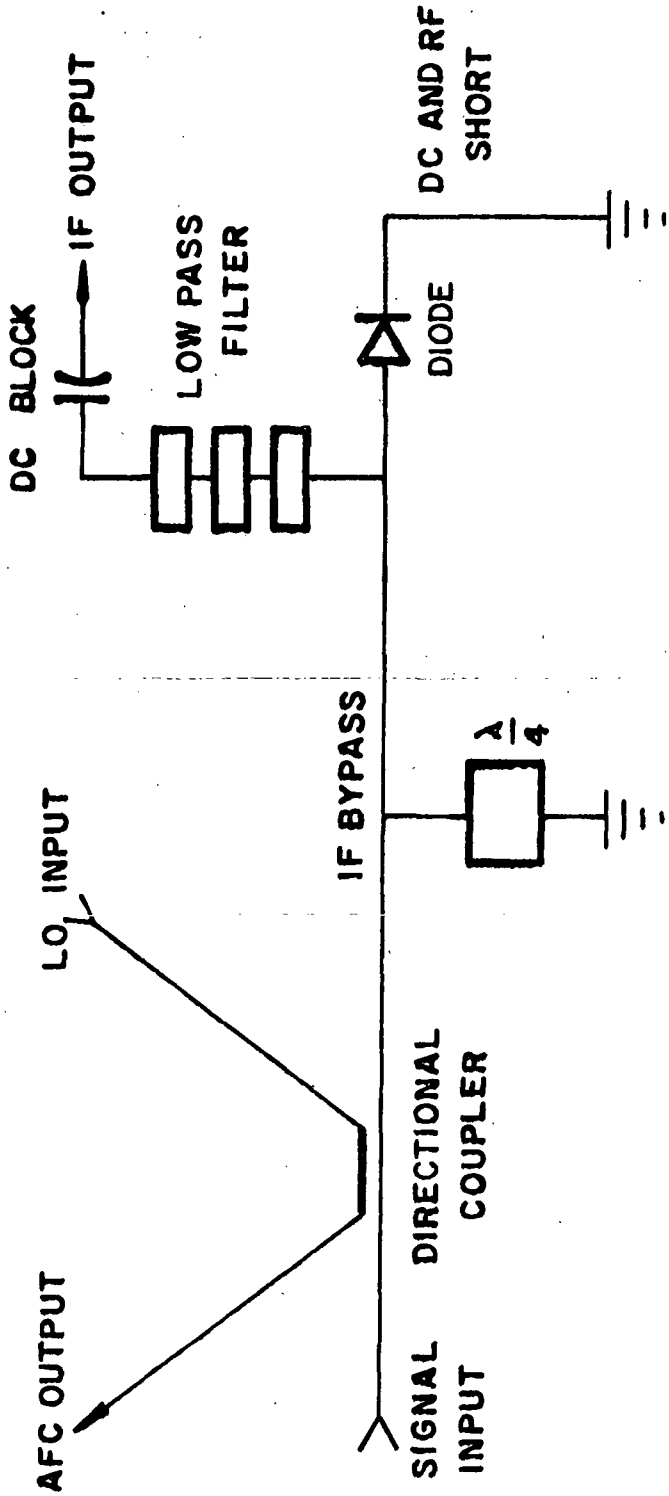


Figure 20. Final Mixer Board Schematic.

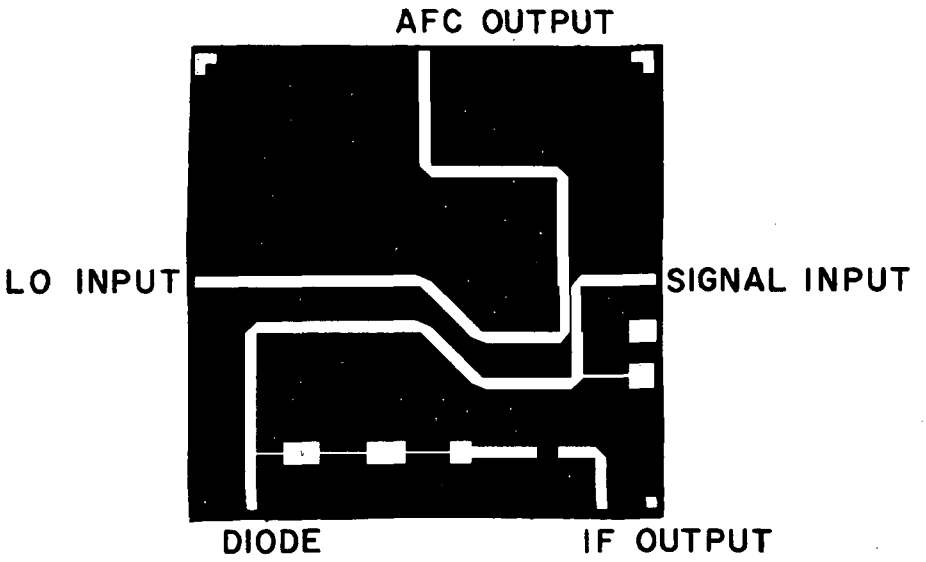


Figure 21. Picture of Final Board Mask.

filters for reasons mentioned above. The IF bypass network serves a dual function; the IF is prevented from being lost out the AFC port (remember that signal and LO ports are X-band waveguide) and a DC return path is provided for the diode.

The coaxial cavity was modified to accommodate both ceramic cartridge and pill-prong packaged diodes. The results found in Chapter 4 show that better performance, both wider bandwidth and lower conversion loss, was achieved with the pill-prong packaged diode. A wider bandwidth is obtained with this package for two reasons. First, the short (approximately .1 in) package requires a shorter resonant cavity and a smaller mean circumference for the coaxial transmission line section which second, results in a higher impedance more easily tuned over a wider bandwidth. The lowpass filter used was described earlier in this section. Significant frontend design characteristics can be found in Table 2. Performance results will be described in Chapter 4.

## 4. PERFORMANCE

One of the ways of characterizing the performance of a down-converter is by specifying its conversion loss, defined as the ratio of power at the signal frequency to that at the IF. For a derivation of conversion loss based on a three-port admittance model for the mixer, see Appendix 7.1. Conversion loss measurements were made on the mixer described in Chapter 3. The circuit used for this measurement is shown schematically in Figure 22.

The measurement procedure consisted of first establishing a reference level of -80dbm on a Tektronix Spectrum Analyzer at one GHz. After establishing the local oscillator at a given power, a signal of known power is introduced to the signal arm of the circuit and the attenuators are adjusted until the signal registers -80dbm on the spectrum analyzer. Since the incident signal power can be calculated immediately from the attenuation settings,and the IF power is -80dbm, the conversion loss is known.

As the LO power is varied the conversion loss changes. The experimental dependence of conversion loss on local oscillator power is shown in Figure 23. Notice that optimum performance occurs at different drive levels for each of the two diodes reported here. All additional narrowband tuning, such as tuning screws for the coax diode cavity and gold epoxy stubs on the MIC were optimized for best performance

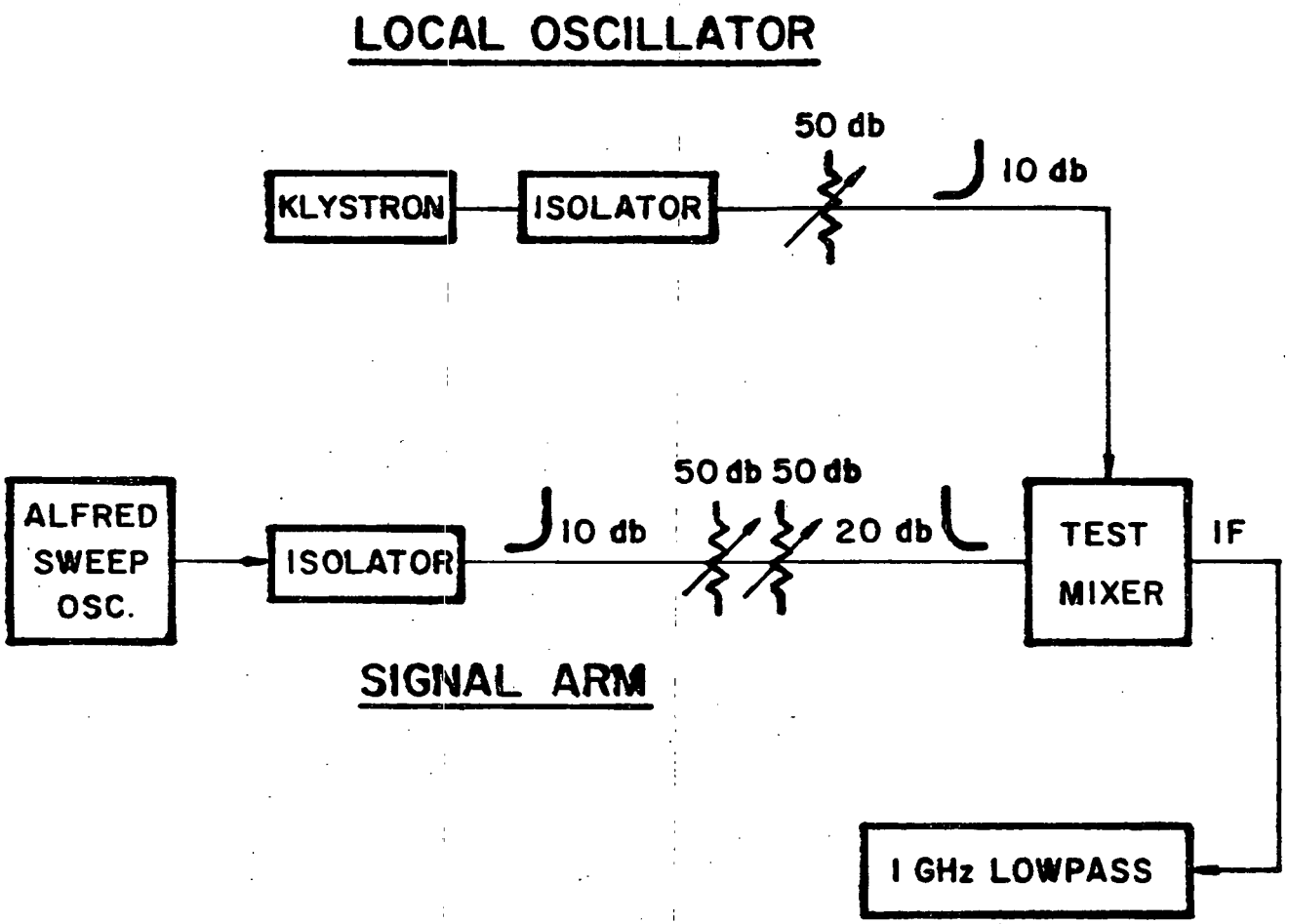


Figure 22. Conversion Loss Measurement Circuit Schematic.

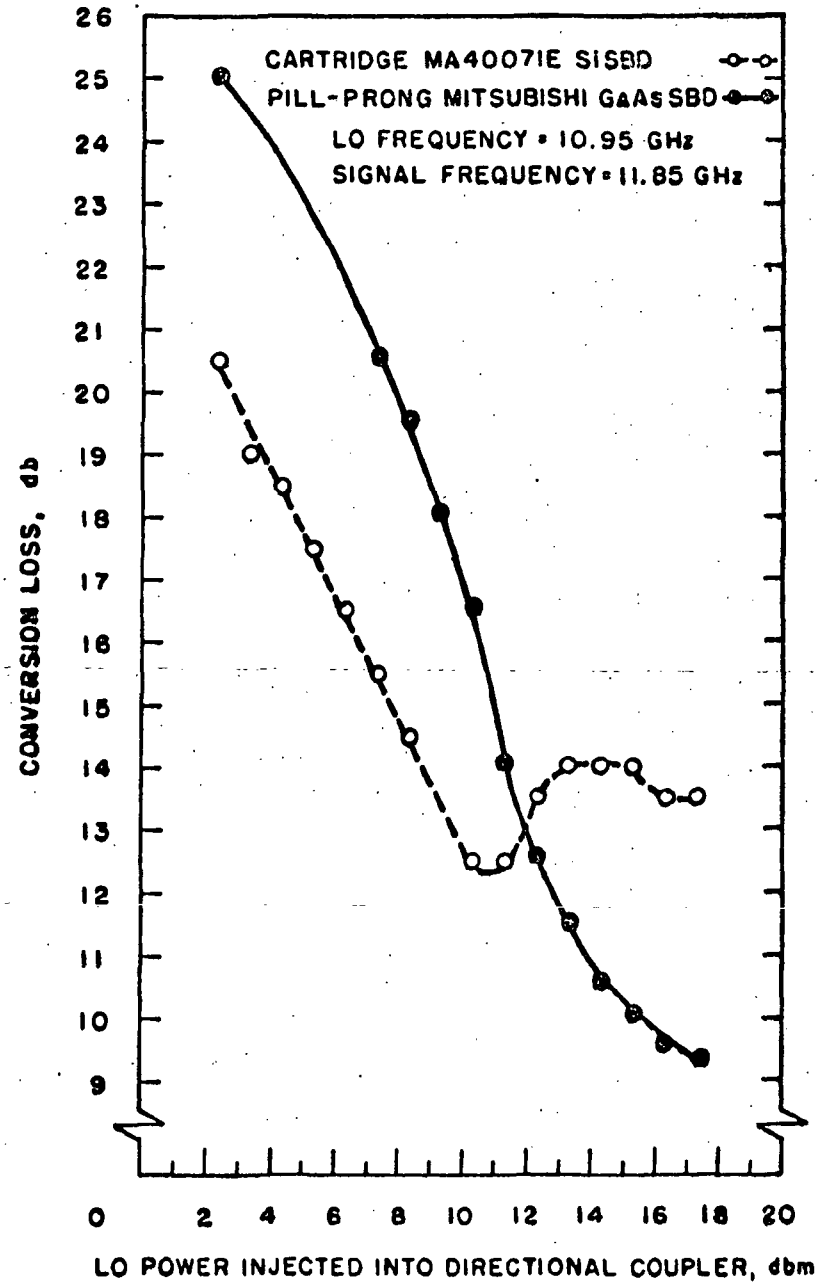


Figure 23. Conversion Loss vs. LO Power.

at this signal frequency and maximum drive level available (17.4dbm injected into the directional coupler). Approximately 8dbm of LO was available at the diode.

The narrowband tuning mentioned above was optimized at a signal frequency of 11.85GHz corresponding to an IF of 900MHz. Figure 24 shows the results of leaving the narrowband tuning unchanged, drive levels as specified in the figure, and varying the signal frequency. The GaAs Mitsubishi Schottky Barrier Diode mounted in a pill-prong package yielded approximately a 275MHz bandwidth with an optimum conversion loss of 9.4db. Referencing the conversion loss to the plane of the diode introduces an improvement of about 1.9db due to mismatch loss, dissipation loss in the microstrip and finally loss due to the directional coupler.

Another quality factor exists that is useful for describing the overall performance of a component or system. This is the noise figure or equivalently the noise temperature. For a derivation of physical sources of noise and system noise figure parameters, see Appendix 7.2. In describing mixer performance specifically, the degradation due to conversion loss can be isolated immediately. The noise figure is given in Appendix 7.2 as $F = L_C N_R$ with all terms defined there. Since the noise ratio, $N_R$, for a GaAs Schottky Barrier diode is for all practical purposes

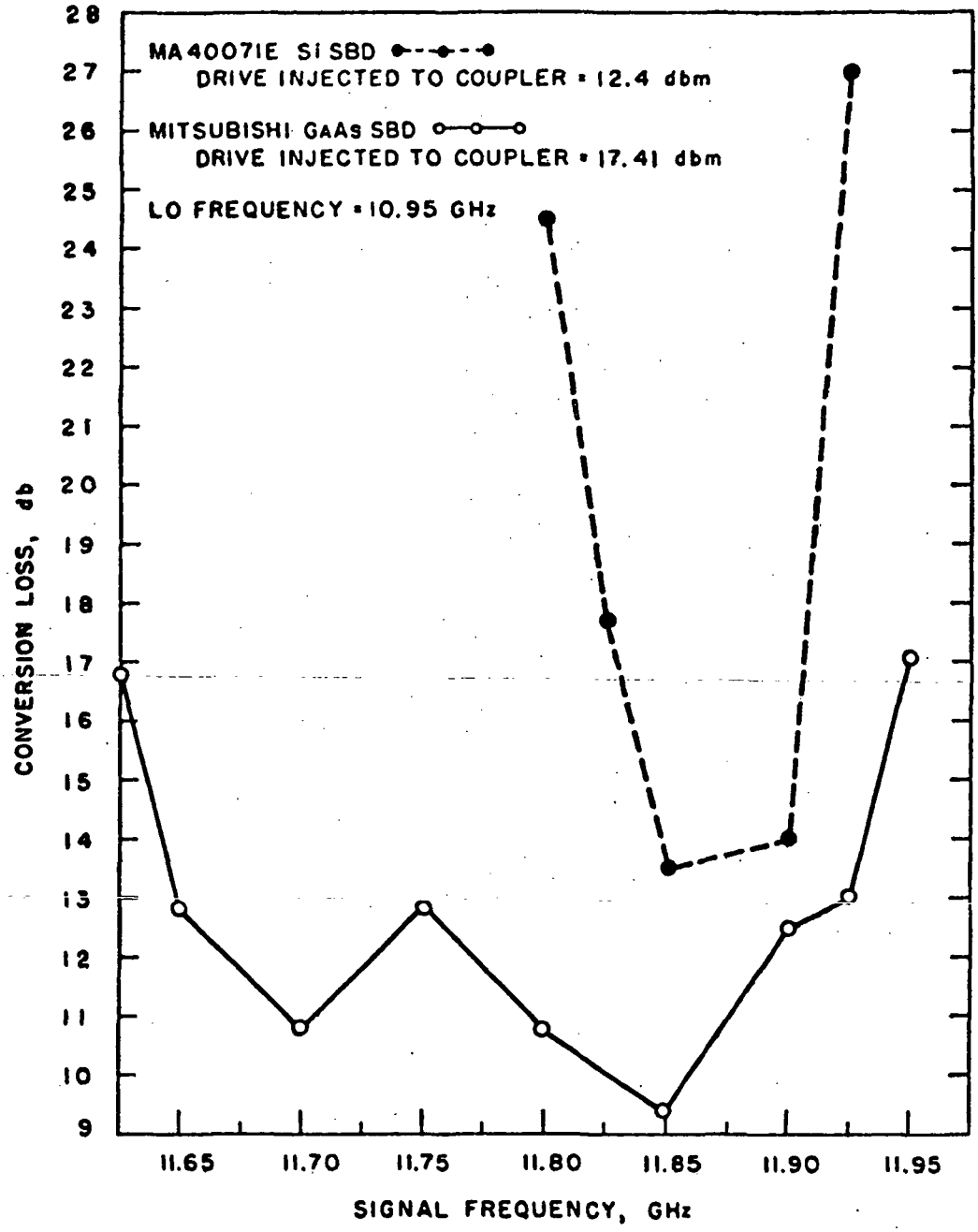


Figure 24. Conversion Loss vs. Signal Frequency.

unity (15), the down-converter noise figure is taken to be equal to the conversion loss for the Mitsubishi results described in Figures 23 and 24. Thus the optimum performance for the down-converter described is a noise figure of 9.4db corresponding to a noise temperature of 2230°K.

# 5. CONCLUSIONS

## 5.1 PRINCIPAL RESULTS

As part of the design of a broadband, X-band down-converter, a number of potentially useful microstrip filters were examined. It was found that the traveling-wave directional filter could serve quite adequately as a diplexer for IFs on the order of 10 per cent of the LO and higher. Good agreement was obtained between experimental and predicted performance for the two coupled ports. The isolated port response was not properly predicted. It is felt that this response might correlate better with experimental work if Standley's analysis is modified to account for external port mismatch. In the present effort, high impedance coupling sections were used and yielded predictable though unsatisfactory results in that the out of band insertion loss to the signal frequency was on the order of 2-3db. However, if the structure is redesigned to preserve a 50Ω impedance throughout, acceptable performance should result.

A quarter-wave 9db directional coupler was used as the diplexer since it presented a lower insertion loss to the signal frequency. Its performance was modeled on the well known scattering matrix for the directional coupler modified to include external port mismatch. Good correlation between experiment and predicted results were obtained for the two coupled ports but the isolated port response was

inaccurate. This might be improved if the reflection coefficient were taken as complex rather than simple magnitudes as now incorporated in the analysis.

Low-pass filters consisting of alternating high and low impedance microstrip sections were fabricated. An analysis based on lossless, dispersionless cascaded transmission line sections was formulated. Good agreement with experiment resulted. The filters designed and tested comprised an even number of elements. To avoid the required impedance transformation, filters with an odd number of elements should be used. This prevents a spurious passband between the second and third harmonic of the cutoff frequency.

Finally, a band-stop filter was fabricated in microstrip. This element was examined to serve as an image enhancement filter. As mentioned earlier, enhancement techniques were not used on this prototype due to an insertion loss to the signal frequency of 1.5db and a higher than anticipated conversion loss and resulting noise figure.

One of the principal features of the mixer itself is the fact that it is single-ended. This configuration was chosen because it is well suited to wideband FM transmission as well as being cost-effective (one diode instead of two or four) and amenable to a design simpler than that for a balanced configuration. The use of waveguide inputs for the signal and LO prevents IF leakage from these ports.

One major change should be made in the layout of the microstrip circuit. Due to mechanical restrictions, the signal port is located over one inch from the diode. The mechanical layout should be such that the signal port is as close as possible to the diode so as to decrease microstrip dissipation.

As mentioned in Section 3.1, it was decided to use field replaceable diodes, either cartridge or pill-prong package. The reasons for this choice are given in that section. Reasonable performance was achieved with a Mitsubishi GaAs Schottky Barrier Diode in a pill-prong package. Complete performance results for the mixer and individual components are summarized in Table 2. A cost estimate for the Washington University down-converter can be found in Table 3.

## 5.2 FUTURE WORK

A number of areas concerned with this work could be pursued further to advantage.

(1) The foremost area in need of improvement is the microstrip fabrication technique used in this project (See Appendix 7.3). Insufficient cleanliness was found to be the major obstacle. This led to poor photoresist and etching, resulting in pinholing and other flaws. Also, it was also found that the contact prints used in the mask production and the etching techniques were not preserving

Table 2. Design Specifications and Performance of 12GHz Down-Converter.

| | | |
|---|---|---|
| Center Frequency | 11.79 | GHz |
| Bandwidth | 275 | MHz |
| LO Frequency | 10.95 | GHz |
| IF Frequency | 840 | MHz |
| Conversion Loss | 9.4 | db |
| Noise Figure (assuming $N_R$ = 1.0) | 9.4 | db |
| Signal/LO Input | X-Band Waveguide | |
| IF/AFC Output | OSM | |
| LO to SIGNAL Isolation | > 11 | db |
| Signal to IF Isolation | > 20 | db |
| LO to IF Isolation | > 28 | db |
| Coupler Directionality | 9 | db |
| Signal to Diode Insertion Loss | 1.9 | db |
| Signal Port VSWR | < 2.3:1 | |

Table 3. Cost Estimate for Down-Converter

Price per Unit in Quantities of 1,000:

| | |
|---|---|
| **Bill of Materials:** | |
| Cast Housing | $ 30.00 |
| Waveguide-Coax-MIC Transitions(2) | 10.00 |
| Diode Holder | 10.00 |
| OSM Connectors(2) | 9.00 |
| GaAs Schottky Barrier Diode | 11.00 |
| Metalized Ceramic Board | 3.45 |
| Miscellaneous Hardware | 1.00 |
| | $ 74.45 |
| **Labor:** | |
| Precision Finish Machining of Casting | $ 25.00 |
| MIC Processing | 5.00 |
| RF Assembly and Test | 10.00 |
| | $ 40.00 |
| TOTAL | $114.45 |
| ESTIMATED SELLING PRICE | $400.00 |

line widths. In sum, the microstrip fabrication technique needs to be brought under control before circuits with exacting tolerances can be realized.

(2) Further work with the traveling-wave directional filter could be pursued in both the analysis and fabrication of a 1.5GHz device. A successful analysis would eliminate the need for numerous experimental iterations on a filter that could be used as the basis of a branching network for the satellite-CATV interconnection system.

(3) The performance obtained with a packaged diode should be adequate when preceded with an RF preamplifier. However, if such an amplifier is not to be used, then a further effort should be pursued using chip or beam-lead diodes. This should result in a low-noise, broadband down-converter since package parasitics necessitate tuning that narrowbands the response and makes it difficult to achieve a low VSWR to the diode. Unpackaged diodes, in general, seem more compatible with the microstrip transmission medium as reported in the literature (see Table 1).

## 6. ACKNOWLEDGEMENT

The author wishes to thank the Center for Development Technology which supported this work through NASA Grant Y/NGL-26-008-054.

# 7. APPENDICES

## APPENDIX 7.1

### Conversion Loss

Referring to Figure 7.1.1, it can be seen that the magnitude of the IF component is a function of the ratio of the slopes of the DC i-v diode characteristic at the negative and positive peaks of the LO voltage. The ratio of the differential impedances decreases as the LO drive level is reduced. Therefore, at moderate drive levels, conversion loss, defined as the ratio of the output power at the IF to that of the input power at the signal frequency, is inversely proportional to the drive level (30).

Although mixing itself is a function of the nonlinearity of the crystal, a linear relation exists between RF input power and IF output power if the LO level is held constant and is orders of magnitude larger than the input signal power. This relationship holds because the voltage-current relationships responsible for conversion are functions of the differentials of the DC characteristics.

Assume that the performance of a mixer can be adequately predicted by modeling the device as a three-port, namely the signal, image and IF ports (30). For a four-port analysis, including the sum components, see Reference 31. Given the symmetry argument of Torrey and Whitmer (31), the voltage current equations for the three port mixer can be specified as follows:

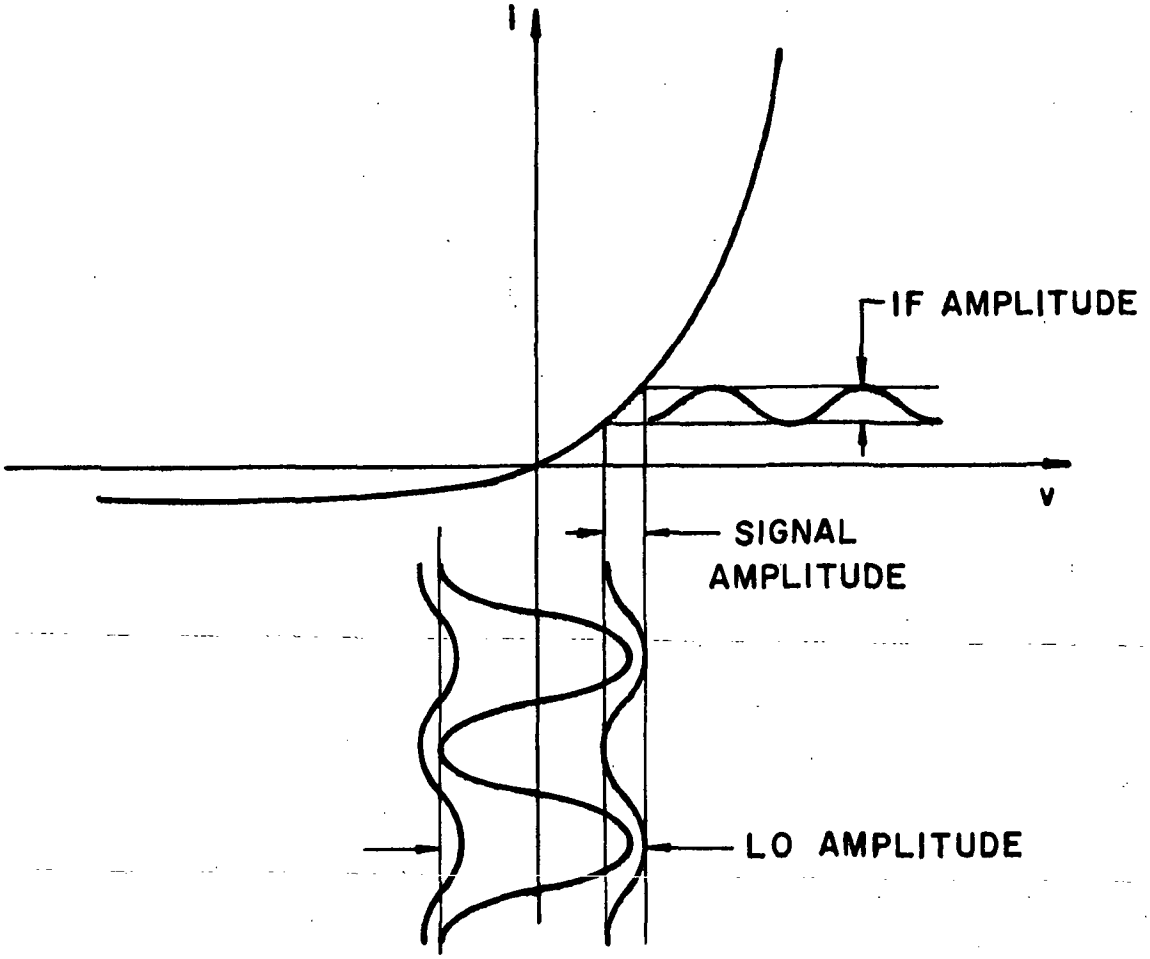


Figure 7.1.1. Magnitude of the IF Component.

$$
\begin{aligned}
i_\alpha &= y_{\alpha\alpha}e_\alpha + y_{\alpha\beta}e_\beta + y_{\alpha\gamma}e^*_\gamma \\
i_\beta &= y_{\beta\alpha}e_\alpha + y_{\beta\beta}e_\beta + y^*_{\beta\alpha}e^*_\gamma \\
i_\gamma &= y^*_{\alpha\gamma}e_\alpha + y^*_{\alpha\beta}e_\beta + y^*_{\alpha\alpha}e^*_\gamma
\end{aligned}
\qquad (7.1.1)
$$

where $\alpha$, $\beta$, and $\gamma$ refer to signal, IF and image components respectively.

It should be noted that the reduction of the above system of equations is based on several qualifying assumptions:

(1) Torrey and Whitmer's analysis relies on the fact that the mixer cannot distinguish between the image and the signal. This does not hold for a high IF since the match would vary widely over a 2:(IF) bandwidth.

(2) The theory also presupposes that the IF and DC components cannot be distinguished, again, obviously untrue for a high IF.

(3) It is also assumed that the IF self-admittance, $y_{\beta\beta} = \mathrm{Re}\ y_{\beta\beta}$, is real.

If the image terminals are connected, independently of the signal terminals, to an external admittance $y_\gamma$, then

$$
\frac{i_\gamma}{e_\gamma} = -y_\gamma \qquad (7.1.2)
$$

Substituting this equation into Equation (7.1.1) and eliminating $e_\gamma$ and $i_\gamma$ between the equations yields the following results for the signal and IF voltage-current relations:

$$i_\alpha = Y_{\alpha\alpha}e_\alpha + Y_{\alpha\beta}e_\beta \tag{7.1.3}$$

$$i_\beta = Y_{\beta\alpha}e_\alpha + Y_{\beta\beta}e_\beta \tag{7.1.4}$$

where

$$Y_{\alpha\alpha} = y_{\alpha\alpha} - \frac{y_{\alpha\gamma}y^*_{\alpha\gamma}}{y^*_\gamma + y^*_{\alpha\alpha}} \tag{7.1.5}$$

$$Y_{\alpha\beta} = y_{\alpha\beta} - \frac{y_{\alpha\gamma}y^*_{\alpha\beta}}{y^*_\gamma + y^*_{\alpha\alpha}} \tag{7.1.6}$$

$$Y_{\beta\alpha} = y_{\beta\alpha} - \frac{y_{\beta\alpha}y^*_{\alpha\gamma}}{y^*_\gamma + y^*_{\alpha\alpha}} \tag{7.1.7}$$

$$Y_{\beta\beta} = y_{\beta\beta} - \frac{y_{\beta\alpha}y^*_{\alpha\beta}}{y^*_\gamma + y^*_{\alpha\alpha}} \tag{7.1.8}$$

Equations (7.1.5) through (7.1.8) show the dependence of the signal and IF parameters on the image termination. The conversion loss, signal input admittance and IF output admittance can be specified in terms of Equations (7.1.3) and (7.1.4) if the signal generator admittance and IF load admittance are also specified.

The signal input admittance $Y_\alpha$, for an IF load admittance $y_\beta$, is:

$$(Y_{\alpha\alpha} - Y_\alpha)e_\alpha + Y_{\alpha\beta}e_\beta = 0 \tag{7.1.9}$$

$$Y_{\beta\alpha}e_\alpha + (Y_{\beta\beta} + y_\beta)e_\beta = 0 \tag{7.1.10}$$

where $Y_\alpha = i_\alpha/e_\alpha$ and $y_\beta = -i_\beta/e_\beta$

Solving for $Y_\alpha$ and $Y_\beta$ yields

$$Y_\alpha = Y_{\alpha\alpha} - \frac{Y_{\alpha\beta}Y_{\beta\alpha}}{y_\beta + Y_{\beta\beta}} \tag{7.1.11}$$

$$Y_\beta = Y_{\beta\beta} - \frac{Y_{\alpha\beta}Y_{\beta\alpha}}{Y_{\alpha\alpha} + y_\alpha} \tag{7.1.12}$$

Equations (7.1.11) and (7.1.12) point out an important fact about mixer circuit design, namely, that RF and IF matching conditions are not independent.

Torrey and Whitmer (31) have shown that for a silicon device, assuming that a time zero exists such that the electric field at the barrier is an even function of time,

$$|Y_{\alpha\beta}| = |Y_{\beta\alpha}| \tag{7.1.13}$$

This reciprocity states that the conversion efficiency from RF to IF equals that from IF to RF power.

The output power of the mixer is $\mathrm{Re}(-\frac{1}{2}i_\beta e_\alpha^*)$. Since the input power is $\mathrm{Re}\,(\frac{1}{2}i_\alpha e_\alpha^*)$, the conversion loss is

$$L = \frac{-\mathrm{Re}(\frac{1}{2}i_\alpha e_\alpha^*)}{\mathrm{Re}(\frac{1}{2}i_\beta e_\beta^*)} \tag{7.1.14}$$

and from Equations (7.1.11) and (7.1.12),

$$L = \frac{G_\alpha}{g_\beta}\left|\frac{e_\alpha}{e_\beta}\right|^2 \tag{7.1.15}$$

where $G_\alpha$ and $g_\beta$ are the conductances of $Y_\alpha$ and $y_\beta$, respectively.

Using Equations (7.1.9) and (7.1.10) to solve for $|e_\alpha/e_\beta|$ and Equations (7.1.11) and (7.1.12) to determine $G_\alpha$ results in:

$$L = \frac{G_{\alpha\alpha} - \mathrm{Re}\left(\frac{Y_{\alpha\beta}Y_{\beta\alpha}}{Y_{\beta\beta}+y_\beta}\right)|Y_{\beta\beta} + y_\beta|^2}{g_\beta|Y_{\beta\alpha}|^2} \qquad (7.1.16)$$

Using $Y = G + jB$ and rewriting the above we have:

$$L = \frac{G_{\alpha\alpha}}{g_\beta|Y_{\beta\alpha}|^2}[(G_{\beta\beta} + g_\beta)^2 - \frac{G_{\alpha\beta\beta\alpha}}{G_{\alpha\alpha}}(G_{\beta\beta} + g_\beta) + (B_{\beta\beta} + b_\beta)^2 - \frac{B_{\alpha\beta\beta\alpha}}{G_{\alpha\alpha}}(B_{\beta\beta} + b_\beta)] \qquad (7.1.17)$$

Maximum power conversion is obtained when the IF load admittance is chosen so as to minimize the loss L. This requires the minimization of the two orthogonal quantities $g_\beta$ and $b_\beta$. Since $b_\beta$ can take on any value $(-\infty,\infty)$, L will have a minimum value when

$$(B_{\beta\beta} + b_\beta)^2 - \frac{B_{\alpha\beta\beta\alpha}}{G_{\alpha\alpha}}(B_{\beta\beta} + b_\beta) \qquad (7.1.18)$$

is a minimum. Taking the derivative of the above expression with respect to $(B_{\beta\beta} + b_\beta)$ and setting the result equal to zero yields:

$$(B_{\beta\beta} + b_\beta) = \frac{B_{\alpha\beta\beta\alpha}}{2G_{\alpha\alpha}} \qquad (7.1.19)$$

Repeating the above procedure for the other variable, $g_\beta$:

$$g_\beta = \left\{G_{\beta\beta}^2 - \frac{G_{\alpha\beta\beta\alpha}G_{\beta\beta}}{G_{\alpha\alpha}} - \left(\frac{B_{\alpha\beta\beta\alpha}}{2G_{\alpha\alpha}}\right)^2\right\}^{1/2} \qquad (7.1.20)$$

From Equations (7.1.19) and (7.1.20), the optimum load admittance is:

$$y_\beta = \left[ G_{\beta\beta}^2 - \frac{G_{\alpha\beta\beta\alpha} G_{\beta\beta}}{G_{\alpha\alpha}} - \left( \frac{B_{\alpha\beta\beta\alpha}}{2G_{\alpha\alpha}} \right)^2 \right]^{1/2} + j \frac{(B_{\alpha\beta\beta\alpha} - B_{\beta\beta})}{2G_{\alpha\alpha}} \qquad (7.1.21)$$

yielding a minimum loss:

$$L = \frac{G_{\alpha\alpha}}{|Y_{\beta\alpha}|^2} 2 \left\{ G_{\beta\beta} - \frac{G_{\alpha\beta\beta\alpha}}{2G_{\alpha\alpha}} + \left[ G_{\beta\beta}^2 - \frac{G_{\alpha\beta\beta\alpha}}{G_{\alpha\alpha}} G_{\beta\beta} - \left( \frac{B_{\alpha\beta\beta\alpha}}{2G_{\alpha\alpha}} \right)^2 \right]^{1/2} \right\} \qquad (7.1.22)$$

Manipulating the above expression gives:

$$L = \left| \frac{Y_{\alpha\beta}}{Y_{\beta\alpha}} \right| \left( \frac{1 + \sqrt{1 - \varepsilon}}{1 - \sqrt{1 - \varepsilon}} \right) \qquad (7.1.23)$$

where

$$\varepsilon = \frac{2|Y_{\alpha\beta}Y_{\beta\alpha}|}{2G_{\alpha\alpha}G_{\beta\beta} - G_{\alpha\beta\beta\alpha} + |Y_{\alpha\beta}Y_{\beta\alpha}|}$$

The quantity $\varepsilon$ is called the impedance loss and can be determined from direct measurement. The above loss will be equal to that measured by direct means only if reciprocity holds, i.e., $|Y_{\alpha\beta}| = |Y_{\beta\alpha}|$.

The analysis of the mixer as a linear circuit suggests examining the specific dependence of the input admittance as a function of the load admittance. This can be done by connecting the IF output terminals to a pure susceptance adjustable to all values $(-\infty,\infty)$. Also let the mixer have RF matching such that the signal admittance is real. From Equations (7.1.9) and (7.1.10),

$$Y_{SC} = G_{SC} = G_{\alpha\alpha} \tag{7.1.24}$$

Adjusting the load susceptance to maximize the input admittance mismatch yields:

$$Y_{OC} = G_{\alpha\alpha} - \frac{Y_{\alpha\beta}Y_{\beta\alpha}}{G_{\beta\beta}+j(B_{\beta\beta}+b_{\beta})} \tag{7.1.25}$$

Expressing the above mismatch as a modular reflection coefficient:

$$|\Gamma| = \left|\frac{Y_{OC} - Y_{SC}}{Y_{OC} + Y_{SC}}\right| = \left|\frac{-Y_{\alpha\beta}Y_{\beta\alpha}}{2G_{\alpha\alpha}G_{\beta\beta} + G_{\alpha\beta\beta\alpha} + j2G_{\alpha\alpha}(B_{\beta\beta} + b_{\beta})}\right| \tag{7.1.26}$$

and

$$|\Gamma|^2 = \frac{(G_{\alpha\beta\beta\alpha})^2 + (B_{\alpha\beta\beta\alpha})^2}{(2G_{\alpha\alpha}G_{\beta\beta} - G_{\alpha\beta\beta\alpha})^2 + [2G_{\alpha\alpha}(B_{\beta\beta} + b_\beta) - B_{\alpha\beta\beta\alpha}]^2} \tag{7.1.27}$$

The maximum mismatch loss is found by differentiating $|\Gamma|^2$ with respect to $(B_{\beta\beta} + b_\beta)$ and setting this result equal to zero. This results in:

$$B_{\beta\beta} + b_\beta = \frac{B_{\alpha\beta\beta\alpha}}{2G_{\alpha\alpha}} \tag{7.1.28}$$

which is identical to that required for minimizing the conversion loss. Using this value in Equation (7.1.25) gives:

$$Y_{OC} = G_{\alpha\alpha} - \frac{G_{\alpha\beta\beta\alpha} + jB_{\alpha\beta\beta\alpha}}{G_{\beta\beta} + j\frac{B_{\alpha\beta\beta\alpha}}{2G_{\alpha\alpha}}} \tag{7.1.29}$$

Choosing the position of the input terminals so as to make $Y_{OC}$ real makes the imaginary part of Equation (7.1.29) equal to zero.

$$G_{\beta\beta}G_{\alpha\beta\beta\alpha} - \frac{B_{\alpha\beta\beta\alpha}G_{\alpha\beta\beta\alpha}}{2G_{\alpha\alpha}} = 0 \tag{7.1.30}$$

This can be so if and only if:

$$2G_{\alpha\alpha}G_{\beta\beta} = G_{\alpha\beta\beta\alpha} \quad \text{or} \quad B_{\alpha\beta\beta\alpha} = 0 \tag{7.1.31}$$

The first condition yields an $\varepsilon > 1$ and is therefore non-physical since the crystal is passive. The second condition gives:

$$Y_{OC} = G_{\alpha\alpha} - \frac{G_{\alpha\beta\beta\alpha}}{G_{\beta\beta}} = G_{OC} \qquad (7.1.32)$$

From Equations (7.1.24) and (7.1.32) we have:

$$\frac{G_{OC}}{G_{SC}} = 1 - \frac{G_{\alpha\beta\beta\alpha}}{G_{\alpha\alpha}G_{\beta\beta}} \qquad (7.1.33)$$

Since $G_{OC}/G_{SC} = 1 - \varepsilon$, the expression for the loss is:

$$L = \left|\frac{Y_{\alpha\beta}}{Y_{\beta\alpha}}\right| \frac{1 + \sqrt{G_{OC}/G_{SC}}}{1 - \sqrt{G_{OC}/G_{SC}}} \qquad (7.1.34)$$

As mentioned above, the reciprocity factor is $|Y_{\alpha\beta}/Y_{\beta\alpha}| = 1$ for silicon devices.

Pound (30) derives the expression for the characteristic impedance of the mixer as being $\sqrt{G_{SC}G_{OC}}$. Given that the RF tuning is matched such that $\sqrt{G_{SC}G_{OC}}$ corresponds to a matched input, then variations in the IF load susceptance will result in sweeping out a circle on a Smith Chart, centered at the origin. The diameter will be inversely proportional to the minimum loss, i.e., a 0 db minimum conversion loss results in a purely susceptive input admittance, lying on the outer diameter of the Smith Chart. An arbitrary load admittance results in a point internal to this circle, with the center point corresponding to an optimum load admittance.

The IF amplifier input circuit is chosen to minimize the noise figure compatible with the bandwidth and gain desired, and not necessarily to optimize the signal match to the mixer diode. However, the mixer tuning should be

such that the characteristic admittance of the mixer is matched to that of the signal generator, since this minimizes conversion loss. That is, optimum IF loading should be used when tuning the mixer and not the input admittance of the IF strip.

Similarly, the IF admittance can be shown to be dependent on the signal admittance. In a completely analogous fashion it is found that:

$$Y_{SC\alpha} = G_{\beta\beta} = G_{SC\alpha} \tag{7.1.35}$$

$$Y_{OC} = G_{\beta\beta} - \frac{G_{\alpha\beta\beta\alpha}}{G_{\alpha\alpha}} = G_{OC\alpha} \tag{7.1.36}$$

Finally, the similar loss term is:

$$L_Z = \frac{1+\sqrt{G_{OC\alpha}/G_{SC\alpha}}}{1-\sqrt{G_{OC\alpha}/G_{SC\alpha}}} \tag{7.1.37}$$

Note that if the signal generator is matched to the diode, the IF admittance will be the characteristic admittance of the IF terminals.

Due to the symmetry between the signal and image frequencies in Equation (7.1.1), the impedance loss of the converter in terms of the IF conductance measured with the image terminals open and short circuited is:

$$L_Z = \frac{1+\sqrt{G_{OC\gamma}/G_{SC\gamma}}}{1-\sqrt{G_{OC\gamma}/G_{SC\gamma}}} \tag{7.1.38}$$

This is the minimum loss that could be obtained if the roles of the signal and image terminals were interchanged.

## APPENDIX 7.2

### Noise Sources and System Noise Parameters

In Section 7.1, conversion loss was given as the power expended in conversion from RF to the IF. There is, however, a quality factor used to characterize not only a down-converter, but also other devices, which includes the effect of conversion loss. This is the noise figure or, equivalently, the noise temperature. Before looking at noise figure itself, consider the origin of noise.

The random nature of electronic motion in a conductor resulting from thermal agitation gives rise to an open-circuit, Gaussian distributed voltage known as Thermal or Johnson Noise. The frequency components of the noise are distributed throughout the spectrum and thus it is referred to as white noise.

The discrete and random nature of the electrons arriving at the metal in a Schottky barrier leads to what is commonly known as shot noise. Since the mean free path of the electron is larger than the barrier width, collision and space charge within the barrier can be overlooked. Torrey and Whitmer have shown that the mean square noise current due to DC excitation is given by (31):

$$\overline{i^2} = 2 e I \Delta f \qquad (7.2.1)$$

where:

e = electronic charge.

I = diode current = $I_1 + I_2$ = electron current from semiconductor → metal and metal → semiconductor.

$\Delta f$ = bandwidth of interest.

An actual diode has distributed contact potential as opposed to a uniform potential for the entire junction area. Each of these in turn leads to a different spreading resistance. The barrier then consists of a number of $r_k$'s in shunt as in Figure 7.2.1.

Consider the uniform contact potential of the ideal case first. The noise power available from the barrier is:

$$P_B = \frac{1}{2} e I R \Delta f \qquad (7.2.2)$$

when R = dV/dI = differential barrier resistance.
Adding the noise power $kT\Delta f$ due to the spreading resistance, the total noise power is:

$$P = \frac{(1/2)e IR^2 + kTr}{R + r} \Delta f \qquad (7.2.3)$$

The noise temperature is then defined as the ratio of P to $kT_o\Delta f$ which implies that the noise temperature is:

$$t = \frac{\frac{e}{2kT_o} IR^2 + r(\frac{T}{T_o})}{R + r} \qquad (7.2.4)$$

Electron currents traversing a uniform contact potential barrier are given by the sum current (31):

$$I = A[e^{+e\beta V/kT} + e^{-e(1-\beta)V/kT}] \qquad (7.2.5)$$


a) IDEAL CASE

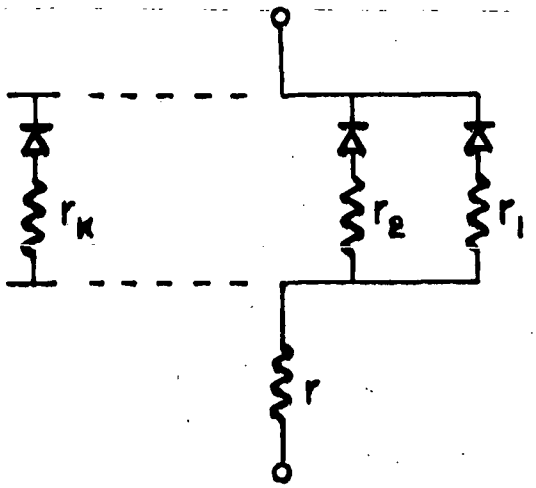


b) NON-IDEAL DISTRIBUTED CONTACT POTENTIAL

Figure 7.2.1. Diode Contact Potential.

where:

A = constant used to fit the i-v characteristic.

V = voltage across the barrier.

β = a parameter that includes the effects of the image force and tunneling in reducing the effective barrier height.

The available barrier shot noise power is given by

$$P_B = \frac{(\frac{1}{2}kT\Delta f)(1 + e^{-eV/kT})}{\beta + (1-\beta)e^{-eV/kT}} \qquad (7.2.6)$$

Consider then the shot noise power in three special cases.

(1) $V = 0$ $\qquad P_B = kT\Delta f$

(2) $V << 0$ $\qquad P_B = \frac{1}{2}\frac{kT\Delta f}{1-\beta}$

(3) $V >> 0$ $\qquad P_B = \frac{1}{2}\frac{kT\Delta f}{\beta}$

Since $\beta \approx 1$, the noise temperature should be about 1/2 in the forward direction, unity at $V = 0$, and large in the reverse direction. Here $\beta$ = constant, but in reality, $\beta$ decreases with increasing voltage. Therefore, in the forward direction, the noise temperature should decrease from unity and later increase, while in the reverse direction, it should get large rapidly.

Looking at a non-ideal distributed contact potential, assume that $V < kT/e$. In this case, the local spreading resistances are small compared with the barrier resistance and the noise power due to the barrier is the principal

source of noise. Taking the discrete spread of contact potential into account,

$$P_B = \frac{1}{2} kT\Delta f \sum_k \frac{R}{\rho_k} \frac{1 - e^{-eV/kT}}{\beta_k + (1-\beta_k)e^{-eV/kT}} \qquad (7.2.7)$$

where

$\rho_k$ = differential resistance.

$\beta_k$ = $k^{th}$ value of $\beta$.

$R = (\sum_k \frac{1}{\rho_k})^{-1}$ = total differential barrier resistance.

If the voltage V >> kT/e, then three possibilities exist. First define (31) overloaded resistance as the case occurring when an electron gains more energy than kT from the field in one free path length. The three cases are:

(1) No overloading and mean free path << radius, a, of an area of uniform contact potential. This leads to localized spreading resistances that are ohmic and contribute a noise power $kT\Delta f$.

(2) In the second case, assume overloading such that the mean free path $\ell$ << a. In this case, the contact is non-ohmic and the noise power for the $k^{th}$ spot is $\frac{\ell}{a} e\, i_k\, \Delta f$.

(3) In the third case of overloading, $\ell$ > a and no collisions occur in the local spreading resistance resulting in noise power due to barrier shot noise alone. The total noise power is then given by:

$$P = \frac{RP_B + rkT\Delta f}{R + r} \qquad (7.2.8)$$

The general expression ($P_B = \frac{1}{2}$ e IR $\Delta$f) should hold even for the more general distributed case for V < kT/e and for the overloaded case when a < $\ell$.

The difference between the measured noise and the predicted shot and thermal noise is known as flicker or "1/f" noise reflecting this quantity's inverse dependence on frequency. Several sources for the 1/f noise have been proposed (32). One approach assumes that a superposition of shot noise spectra can result in a 1/f distribution if a distribution of time constant is introduced. McWhorter (33) proposes that 1/f noise is a surface phenomenon and arises from fluctuations in the occupancy of the slow surface states which lead to random fluctuations in the surface potential. Petritz (34) says that the local breakdown of barriers, with energy supplied by the electric field, leads to 1/f noise. Starting and healing processes with varying thicknesses of surface oxide would give rise to a 1/f noise spectrum. Bess (35) proposed that 1/f noise is caused by the shifting of the Fermi level and association with edge dislocation densities within the bulk. The model assumes that emission centers occur when edge dislocation lines meet the surface. The actual noise event is the emission of an impurity atom from an emission center. The

impurity atom then diffuses along the surface and may trap one hole or electron in the bulk.

Now that the sources of noise in a mixer diode have been discussed, consider some of the concepts that must be understood when discussing noise. In the above discussion, reference was made several times to the bandwidth, BW, of the system. More precisely, the equivalent noise bandwidth is the quantity needed. This is the bandwidth found by computing the area under an actual gain vs. frequency curve and converting to a flat-top pass band of equal area with a height equal to that of the actual maximum gain. In general, the noise BW is very nearly equal to the 3db bandwidth for a multistage amplifier (36).

The noise temperature of a system is defined as the temperature of a passive system having an available noise power per unit bandwidth equal to that of the actual port at a standard temperature, usually 290°K (36). The total output noise for a single response receiver can then be expressed as follows:

$$N_{T_o} = GkB(T_i + T_e) \qquad (7.2.9)$$

where:

G = gain response.

k = Boltzmann's constant.

B = noise bandwidth.

$T_i$ = noise temperature of the input termination.

$T_e$ = effective input noise temperature of the receiver.

For a multiple response receiver, the output noise is expressed by:

$$\sum_j G_j \, kB_j(T_{ij} + T_e) \tag{7.2.10}$$

where $j$ is the multiplicity of responses.

Now consider two units operating in cascade. For simplicity, the bandwidths are assumed to be identical. The total output noise is given by:

$$N_{T_o} = G_1 G_2 kB(T_i + T_{e12}) \tag{7.2.11}$$

where $T_{e12}$ is the overall input noise of the two units in cascade.

The output noise power of the second amplifier can then be divided as follows:

$$N_{T_o} = G_2 kBT_{e2} + G_2[G_1 kB(T_{i1} + T_{e1})] \tag{7.2.12}$$

Solving the above two equations for the overall effective input noise temperature for the combination:

$$T_{e12} = T_{e1} + T_{e2}/G_1 \tag{7.2.13}$$

Similarly, for n units in cascade,

$$T_{e1,2,\ldots,n} = T_{e1} + \frac{T_{e2}}{G_1} + \frac{T_{e3}}{G_1 G_2} + \ldots + \frac{T_{en}}{G_1 G_2 \ldots G_{n-1}} \tag{7.2.14}$$

From the above it can be seen that the noise temperature of a cascaded system is dominated by the early stages. Specifically, if a loss, L, is introduced before an amplifier of temperature $T_e$, then, since the effective input noise temperature of a matched pad is $T_e = (L-1)T_L$ (see Reference 36), the total effective input noise temperature is given by:

$$T_{e12} = (L - 1)\, T_L + LT_e \tag{7.2.15}$$

The effective input noise temperature may be measured directly without information concerning bandwidth, gain, or whether or not multiple responses exist (36). Given the hot and cold temperature of a noise source, and the difference in output levels of the device with the above noise source as an input, the Y factor, results in:

$$T_e = \frac{T_i L - Y T_{i_L}}{Y - 1} \tag{7.2.16}$$

The other and equivalent quantity necessary for describing the ultimate performance of a system is the noise figure. The IEEE definition for the noise figure (F) of linear receivers is:

$$F = \frac{N_{T_o} \text{ (when } T_i = 290°K \text{ at all frequencies)}}{G_S k\, 290\, B_S} \tag{7.2.17}$$

Noise figure has also been defined using signal to noise ratios by H. T. Friis (36) as:

$$F = \frac{(S_i/k\ 290\ B)}{(S_o/N_{T_o})} = \frac{(S_i/k\ 290\ B)}{S_o} N_{T_o} \tag{7.2.18}$$

where

$S_i, S_o$ = input, output signal power respectively.

$B$ = bandwidth assumed here to be equal for signal and noise.

Since $S_o = G_S S_i$, Equation (7.2.18) reduces to:

$$F = \frac{N_{T_o}}{G_S k\ 290\ B} \tag{7.2.19}$$

as in the IEEE definition. Equation (7.2.18) simplifies only for the case of a linear receiver, i.e., signal gain, $G_S = G_N$ noise gain (36).

It should be noted that the noise figure of a receiver or amplifier depends on the use of the system. For instance, assume that a receiver has two equal responses, i.e., signal and image, having the same gain, G, and bandwidth, B. When used in a radar system with the single side-band signal appearing in the signal band only, the noise figure is given by:

$$F_1 = \frac{N_{T_o}(\text{when } T_i = 290 \text{ at all frequencies})}{G\ k\ 290\ B} \tag{7.2.20}$$

Used in a system where a double-sideband signal occurs in both bands, as the signal and image responses:

$$F_B = \frac{N_{T_o}(\text{when } T_i = 290 \text{ at all frequencies})}{G\ k\ 290\ (2B)} \tag{7.2.21}$$

Since the output noise has not changed in either case, it is seen that the receiver used in the radar application has twice the noise figure as when used in a broadband

application, such as radio astronomy. Note that, in contrast, the effective input noise temperature mentioned above is a bandwidth-free concept.

In a manner completely analogous to the derivation of the cascaded noise temperature, the cascaded noise figure is given as

$$F = F_1 + \frac{F_2 - 1}{G_1} + \frac{F_3 - 1}{G_1 G_2} + \ldots + \frac{F_n - 1}{\prod_{i=1}^{n-1} G_i} \qquad (7.2.22)$$

where $F_n$ is the noise figure of the $n^{th}$ stage and $G_n$ its gain.

In a single response receiver, the relationship between noise temperature and noise figure is given as:

$$T_e = (F - 1)290 \quad \text{or} \quad F = 1 + \frac{T_e}{290} \qquad (7.2.23)$$

In a multiple-response receiver, the use of the receiver determines its performance. In the broadband case, it can be shown (26) that the noise figure is identical to the above result for a single response receiver. If the signal occurs in one channel only,

$$F_{radar} = \frac{N_{T_o}\ (T_i = 290)}{G_1 k\ 290\ B_1} \qquad (7.2.24)$$

$$= (1 + \frac{T_e}{290})(1 + \frac{G_2 B_2}{G_1 B_1} + \ldots + \frac{G_n B_n}{G_1 B_1})$$

where all quantities are defined as above. In the above work, it was assumed that the input temperature was 290°K.

If the input temperature is not equal to 290°K, say $T_i$, then the output noise is given as:

$$N_{T_o} = G_1 kB[T_i + (F-1)290] \tag{7.2.25}$$

Finally, for the experiments done here, the mixer noise figure is given as:

$$F_M = L_C N_R \tag{7.2.26}$$

where:

$L_C$ = conversion loss of the mixer.

$N_R$ = noise ratio = ratio of mixer effective noise temperature to the standard noise temperature.

The noise figure for the down-converter is:

$$F = L_{RF} + \frac{L_C N_R - 1}{\frac{1}{L_{RF}}} + \frac{F_{if} - 1}{\frac{1}{L_{RF} L_C}} \tag{7.2.27}$$

$$= L_{RF}\, L_C (N_R + F_{if} - 1)$$

where

$L_{RF}$ = input RF losses.

$F_{IF}$ = noise figure of IF amplifier.

All of the above information refers to the spot noise figure, that is, the single frequency noise figure. The average noise figure is given by:

$$\bar{F} = \frac{\int F(f)\, G(f)\, df}{\int G(f)\, df} \tag{7.2.28}$$

## APPENDIX 7.3

### Microstrip Fabrication Technique

#### 7.3.1 Mask Preparation

After the circuit has been designed, the mask is cut (20:1) on Keuffel & Esser's Stabilene Film using an Aristo Coordinatograph.

##### 7.3.1.1 Photoreduction of the Mask

Materials: Nikon 55mm f/3.5 Lens; Kodak High Resolution 2" x 2" Plates.

Procedure: Distance from mask to lens should be set such that image or ground glass screen represents a 20:1 reduction. Focus is set accordingly. Setting the lens at f/5.6, optimum results can be obtained using a 23 second exposure time.

##### 7.3.1.2 Developing the Plates

Materials: Kodak D-19 Developer, Indicator Stop Bath, Rapid Fixer and Photo-Flo 200.

Procedure: Plates should be submerged in the developer for ten minutes; stop bath for ten seconds and one minute in the fixer. Hypo should not be used! Plates should then be washed in 70°F water for five minutes. After rinsing plates in Photo-Flo (one capful/liter water), drying without forced air should take about two hours.

7.3.1.3 Contact Prints - Depending on the type of photo-resist available, positive or negative, contact prints may be required to insure the proper transfer of the desired circuit to the surface of the sample.

Materials: Kodak High Resolution Plates; Enlarger.

Procedure: Enlarger was used as exposing source with height set at 24 inches. Of course, any suitably controlled light source would suffice. The unexposed photographic plate is placed emulsion side up on a black matte surface. The negative exposed plate is placed with the pattern down on the unexposed plate. Intimate contact is insured by placing a heavy glass plate 3/8 inches thick on top of the two photographic plates. Optimum exposure time is 20 seconds. The plate should then be developed as per Section 7.3.1.2. The important thing to note about the contact print process is that it is difficult to preserve line widths. In strict tolerance work, it should be avoided.

7.3.2 Sample Preparation

For the work reported here, Electrotec #SFG-100-250 alumina with chrome-gold plating microstrip boards were used. Some early work was done with vapor-deposition and plating on raw alumina samples. Since even some commercial samples require further plating, that technique will be reported here.

7.3.2.1 Gold Plating

Materials: Sel-Rex "Pura-Gold 125", TCE (Trichlorethylene), 20% $H_2SO_4$, DI (deionized water).

Procedure: The sample should first be cleaned in TCE for 30 seconds, followed by a DI rinse. This is followed by a 30 second rinse in $H_2SO_4$, a DI rinse and immediate immersion in the plating solution. NOTE: The proper potential should exist across the electrodes before immersion. Failure to do this will result in passivation of the surface leading to a poor quality plate. The manufacturer recommends a current density of 3 amps/square foot. For a one inch square plated on both sides, this results in a 41.6 mA current. Gold is deposited at the rate of 1 mil/12.6 minutes. Good results were obtained with the bath maintained at 58°C. Since the ionic concentration is being depleted, bias across the electrodes must periodically be adjusted to maintain a constant current. After removing from the bath, the sample is rinsed in DI.

7.3.2.2 Photoresist

Materials: Kodak Thin Film Resist (KTFR), Trichlorethylene (TCE), Isopropyl Alcohol, KTFR Developer and Thinner, Millipore Filter Holder XX3001200

with Prefilter AP2501000 and Filter NRWP01300; Paasche Airbrush Model H.

Procedure: (a) The sample should first be cleaned by immersing it in TCE and then ultrasonically agitating the sample for five minutes. This is followed by two five-minute periods in isopropyl alcohol, using clean solvent each time.

(b) The sample is then baked in a clean oven at 105°C for 15 minutes.

(c) The photoresist is then prepared in the ratio of two parts KTFR per one part KTFR Thinner. This mixture is then dispensed through a Millipore pre-filter and filter in the amount of one cc per square inch of substrate.

(d) The substrate is then spun at 1800 RPM for 45 seconds.

(e) The sample is then baked again at 105°C for 15 minutes.

(f) The circuit is then exposed on the photoresist using a UV source and an exposure time of 30 seconds.

(g) The circuit is then developed using KTFR developer and an airbrush.

(h) As a final step the sample is heated rapidly to 160°C and removed from the heat immediately.

7.3.2.3 Etching

Materials: Transene Gold Etch, Transene Chrome Etch, Black Wax and TCE solution, TCE, Xylene, DI.

Procedure: The ground plane is first coated with a solution of black wax and TCE. After drying, the sample is placed in a beaker filled with 25cc of gold etch/square inch of gold surface area. Optimum results were obtained using vigorous agitation for 30 minutes, The sample is then rinsed in DI and placed in ten cc of chrome etch/square inch of chrome surface area. The chrome etch is then agitated for about two minutes. Finally, the sample is placed in TCE to remove the black wax from the ground plane.

7.3.2.4 Mounting

Materials: Superior #30 Flux, Indium Indalloy #2 Solder, Epo-tek H41 Gold Epoxy.

Procedure: The mounting block and sample are heated to 300°F. The flux is applied and a small amount of solder is applied evenly to the surface of the mounting block. The sample is then placed on the block and pressed down firmly. The coax-microstrip connectors are attached electronically using the gold epoxy.

## 8. BIBLIOGRAPHY


1. B. A. Newman, J. P. Singh, and F. J. Rosenbaum, "Design of a 12GHz Multicarrier Earth Terminal for Satellite-CATV Interconnection", submitted to NASA, Washington University, St. Louis, Missouri, November 1971.

2. J. P. Singh, "Operating Frequencies for Educational Satellite Services", Memorandum 71-10, Washington University - NASA Program on Application of Communication Satellites to Educational Development, Washington University, St. Louis, Missouri, November 1971.

3. B. B. Lusignan, et al., "The Design and Development of a Low-Cost Microwave Adapter Suitable for Television Reception from High-Power Communications Satellites", NASA Technical Report No. 3682-1, pp. 153-156, October 1970.

4. F. J. Rosenbaum and W. C. Tsai, "Gunn Effect Swept Frequency Oscillator", Proceedings of the IEEE (Letters), 56, pp. 2164-2165, December 1968.

5. W. C. Tsai and F. J. Rosenbaum, "Bias Circuit Oscillations in Gunn Devices", IEEE Transactions on Electron Devices, ED-16, pp. 196-202, February 1969.

6. F. J. Rosenbaum, "Microwave Circuit Design for Wide-Band Tunable Gunn Effect Oscillators", Proceedings of the National Electronics Conference, 25, pp. 176-180, Chicago, Illinois, December 1969.

7. W. C. Tsai, F. J. Rosenbaum, and L. A. MacKenzie, "Circuit Analysis of Waveguide-Cavity Gunn Effect Oscillator", IEEE Transactions on Microwave Theory and Techniques, MTT-18, pp. 808-816, November 1970.

8. W. C. Tsai and F. J. Rosenbaum, "Amplitude and Frequency Modulation of a Waveguide Cavity CW Gunn Oscillator", IEEE Transactions on Microwave Theory and Techniques, op. cit.

9. F. J. Rosenbaum, "Gunn Device Applications", Digest, IEEE 71 International Convention, IEEE Cat. No. 71C8, pp. 522-523, March 1971.

10. E. F. Miller, (Prog. Tech. Mgr.), "Ground Signal Processing System, Summary Reports on Analysis, Design and Cost Estimating", Contract NAS-3-11520, pp. 5-6, June 1970.

11. K. M. Johnson, "X-Band Integrated Circuit Mixer with Reactively Terminated Image", IEEE Transactions on Microwave Theory and Techniques, MTT-16, pp. 388-397, July 1968.

12. L. Napoli and J. Hughes, "Low-Noise Integrated X-Band Receiver", Microwave Journal, 11, pp. 37-42, July 1968.

13. T. H. Oxley, "X-Band Integrated Circuit Receiver", Microwave Journal, 13, pp. 52-55, 1970.

14. J. E. Degenford, et al., "An Integrated X-Band Image and Sum Frequency Enhanced Mixer with 1GHz IF", 1971 International Microwave Symposium Digest, pp. 16-17, May 1971.

15. T. L. Osborne, et al.,"Low Noise Receiving Down-Converter", Bell System Technical Journal, pp. 1651-1663, July-August, 1969.

16. Private communication with Dr. Konishi of NHK Research Lab, Japan.

17. M. R. Barber, "Noise Figure and Conversion Loss of the Schottky Barrier Mixer Diode", IEEE Transactions on Microwave Theory and Techniques, MTT-15, No. 11, November 1967.

18. T. G. Bryant and J. A. Weiss, "Parameters of Microstrip Transmission Lines and of Coupled Paris of Microstrip Lines", IEEE Transactions on Microwave Theory and Techniques, MTT-16, No. 12, pp. 1021-1027, December 1968.

19. H. A. Wheeler, "Transmission Line Properties of Parallel Strips Separated by a Dielectric Sheet", IEEE Transactions on Microwave Theory and Techniques, MTT-13, No. 2, pp. 172-185, March 1965.

20. E. Yamashita and R. Mittra, "Variational Method for the Analysis of Microstrip Lines", IEEE Transactions on Microwave Theory and Techniques, MTT-16, No. 4, April 1968.

21. H. E. Steinhelfer, "An Accurate Calculation of Uniform Microstrip Transmission Lines", IEEE Transactions on Microwave Theory and Techniques, MTT-16, No. 7, July 1968.

22. R. E. Collin, Foundations for Microwave Engineering, McGraw-Hill, New York, 1966.

23. G. L. Matthaei, et al., Microwave Filters, Impedance-Networks, and Coupling Structures, McGraw-Hill, New York, 1964.

24. R. D. Standley, "Analysis of Traveling-Wave Resonator Filters and Associated Networks", Illinois Institute of Technology, Ph.D., 1966.

25. F. S. Coale, "A Traveling-Wave Directional Filter", IRE Transactions on Microwave Theory and Techniques, MTT-4, pp. 256-260, October 1956.

26. R. D. Standley, "Discontinuity Effects in Single Resonator Traveling Wave Filters", IEEE Transactions on Microwave Theory and Techniques, November 1963.

27. K. M. Johnson, "X-Band Integrated Circuit Mixer with Reactivity Terminated Image", IEEE Transactions on Microwave Theory and Techniques, MTT-16, No. 7, July 1968.

28. E. M. T. Jones and J. T. Bolljahn, "Coupled-Strip-Transmission-Line Filters and Directional Couplers", IRE Transactions on Microwave Theory and Techniques, April 1956.

29. M. Katoh and Y. Akaiwa, "4GHz Integrated-Circuit Mixer", IEEE Transactions on Microwave Theory and Techniques, MTT-19, No. 7, pp. 634-637, July 1971.

30. R. V. Pound, Microwave Mixers, MIT Radiation Laboratory Series, Louis N. Ridenour, editor, McGraw-Hill, New York, 1948.

31. H. C. Torrey and C. A. Whitmer, Crystal Rectifiers, MIT Radiation Laboratory Series, L. N. Ridenour, editor, Boston Technical Publishers, Inc., Lexington, Massachusetts, 1964.

32. S. T. Eng, "A New Low 1/f Noise Mixer Diode", Solid State Electronics, Pergamon Press, Great Britain, pp. 55-77, 1965.

33. A. L. McWhorter, MIT Lincoln Laboratory Report No. 80; May 1955.

34. R. L. Petritz, Semiconductor Surface Physics, R. H. Kingston, editor, University of Pennsylvania Press, p. 266, 1957.

35. L. Bess, Physical Review 103, No. 72, 1956.

36. M. W. Mumford and E. H. Scheibe, Noise Performance Factors in Communication Systems, Horizon House-Microwave, Inc., Dedham, Massachusetts, 1968.